LETTER

https://doi.org/10.1038/s41586-019-1426-6

Intercellular interaction dictates cancer cell ferroptosis via NF2–YAP signalling

Jiao Wu[1,2,6], Alexander M. Minikes[2,3,6], Minghui Gao[2,4], Huijie Bian[1], Yong Li[1], Brent R. Stockwell[5], Zhi-Nan Chen[1]* & Xuejun Jiang[2]*

Ferroptosis, a cell death process driven by cellular metabolism and iron-dependent lipid peroxidation, has been implicated in diseases such as ischaemic organ damage and cancer[1,2]. The enzyme glutathione peroxidase 4 (GPX4) is a central regulator of ferroptosis, and protects cells by neutralizing lipid peroxides, which are by-products of cellular metabolism. The direct inhibition of GPX4, or indirect inhibition by depletion of its substrate glutathione or the building blocks of glutathione (such as cysteine), can trigger ferroptosis[3]. Ferroptosis contributes to the antitumour function of several tumour suppressors such as p53, BAP1 and fumarase[4–7]. Counterintuitively, mesenchymal cancer cells—which are prone to metastasis, and often resistant to various treatments—are highly susceptible to ferroptosis[8,9]. Here we show that ferroptosis can be regulated non-cell-autonomously by cadherin-mediated intercellular interactions. In epithelial cells, such interactions mediated by E-cadherin suppress ferroptosis by activating the intracellular NF2 (also known as merlin) and Hippo signalling pathway. Antagonizing this signalling axis allows the proto-oncogenic transcriptional co-activator YAP to promote ferroptosis by upregulating several ferroptosis modulators, including ACSL4 and TFRC. This finding provides mechanistic insights into the observations that cancer cells with mesenchymal or metastatic property are highly sensitive to ferroptosis[8]. Notably, a similar mechanism also modulates ferroptosis in some non-epithelial cells. Finally, genetic inactivation of the tumour suppressor NF2, a frequent tumorigenic event in mesothelioma[10,11], rendered cancer cells more sensitive to ferroptosis in an orthotopic mouse model of malignant mesothelioma. Our results demonstrate the role of intercellular interactions and intracellular NF2–YAP signalling in dictating ferroptotic death, and also suggest that malignant mutations in NF2–YAP signalling could predict the responsiveness of cancer cells to future ferroptosis-inducing therapies.

Cellular metabolism has a crucial role in ferroptosis[1,2]. To study the underlying mechanisms further, we manipulated cellular metabolism by altering the ingredients of culture medium or cell number in culture. Unexpectedly, we observed that cells became more resistant to ferroptosis when approaching high confluence. In HCT116 human colon cancer cells, higher cell confluence conferred resistance to ferroptosis and associated lipid peroxidation, induced by cystine starvation, the cystine transporter inhibitor erastin and the GPX4 inhibitor RSL3 (Fig. 1a, b and Extended Data Fig. 1a–e). Using corresponding pharmacological inhibitors, we confirmed that cells underwent ferroptosis rather than apoptosis or necroptosis under these conditions (Extended Data Fig. 1f, g). Notably, previous published observations also suggest cell-density-dependent ferroptosis: GPX4-null mouse embryonic fibroblasts (MEFs) were able to grow when seeded at high density or as 3D spheroids, but died rapidly after passage at low density[12,13].

To examine whether such dependence on cell density is a general property of ferroptosis, we tested a panel of human epithelial cancer cell lines (Fig. 1c). Most tested cell lines showed cell density dependence, with two exceptions: MDA-MB-231 (MDA231) cells were always sensitive to ferroptosis, whereas BT474 cells were always resistant, regardless of density. To better mimic the in vivo context, we cultured these cells into 3D tumour spheroids. Consistently, erastin triggered more prominent cell death in spheroids formed by MDA231 and H1650 cells (Fig. 1d, e). A possible explanation for this phenomenon is that high cell density more rapidly depletes glutamine (required for cysteine-deprivation-induced ferroptosis[4,14]). However, replenishing glutamine to confluent cells did not restore cell death (Extended Data Fig. 1h).

Cells tend to forge cell–cell contacts with higher cell confluence, and E-cadherin (ECAD) is an important mediator of intercellular contact in epithelial cells[15]. Expression of ECAD correlated with sensitivity to ferroptosis: ECAD was undetectable in MDA231 cells and very low in H1650 cells (Fig. 1f). As cell density increased, ECAD expression increased and became enriched at sites of cell–cell contact in cells that underwent density-dependent ferroptosis; BT474 cells, which are resistant to ferroptosis regardless of confluence, expressed high levels of ECAD even at low cell density (Extended Data Fig. 2a–d). Strong expression of ECAD was detected in spheroids generated from HCT116 cells, but not in those generated from MDA231 cells (Extended Data Fig. 2e). To determine further whether ECAD has a causative role, we tested whether inhibition of ECAD dimerization would sensitize confluent cells to ferroptosis. Indeed, an anti-ECAD antibody that blocks its intercellular dimerization markedly increased the sensitivity of confluent cells to ferroptosis (Extended Data Fig. 2f). ECAD depletion (ΔECAD) rendered confluent HCT116 cells sensitive to ferroptosis (Extended Data Fig. 2g–i). ECAD depletion did not induce expression of N-cadherin (NCAD) in HCT116 cells (Extended Data Fig. 2g). Re-expression of full-length ECAD, but not a truncated mutant lacking the ectodomain (required for intercellular dimerization of ECAD), restored resistance to ferroptosis in ΔECAD cells (Fig. 1g, h and Extended Data Fig. 2j, k).

ECAD-mediated intercellular interaction can signal to the Hippo pathway[16,17], which regulates a plethora of biological events that includes control of proliferation and of organ size[18,19]. The Hippo pathway involves the tumour suppressor NF2 and a kinase cascade consisting of MST1, MST2, LATS1 and LATS2. NF2 has been shown to activate the Hippo signalling pathway by inhibiting CRL4–DCAF1, a ubiquitin ligase complex that promotes proteasomal degradation of LATS1 or LATS2[20,21]. LATS1 and LATS2 phosphorylate the pro-oncogenic transcription co-activator YAP, leading to its nuclear exclusion and inactivation. As expected, as HCT116 cells grew more confluent, increased phosphorylation and decreased nuclear localization of YAP were observed (Extended Data Fig. 3a, b); ECAD knockout or *NF2* RNA interference (RNAi) diminished cell-density-regulated nuclear exclusion of YAP (Extended Data Fig. 3c–g, Supplementary Table 1). To confirm further that YAP is functionally activated under these conditions, we used an 8xGTIIC-luciferase reporter assay that monitors

[1]National Translational Science Center for Molecular Medicine, Department of Cell Biology, School of Basic Medicine, Air Force Medical University, Xi'an, China. [2]Cell Biology Program, Memorial Sloan-Kettering Cancer Center, New York, NY, USA. [3]BCMB Allied Program, Weill Cornell Graduate School of Medical Sciences, New York, NY, USA. [4]The HIT Center for Life Sciences, School of Life Science and Technology, Harbin Institute of Technology, Harbin, China. [5]Department of Biological Sciences, Department of Chemistry, Columbia University, New York, NY, USA. [6]These authors contributed equally: Jiao Wu, Alexander M. Minikes. *e-mail: znchen@fmmu.edu.cn; jiangx@mskcc.org

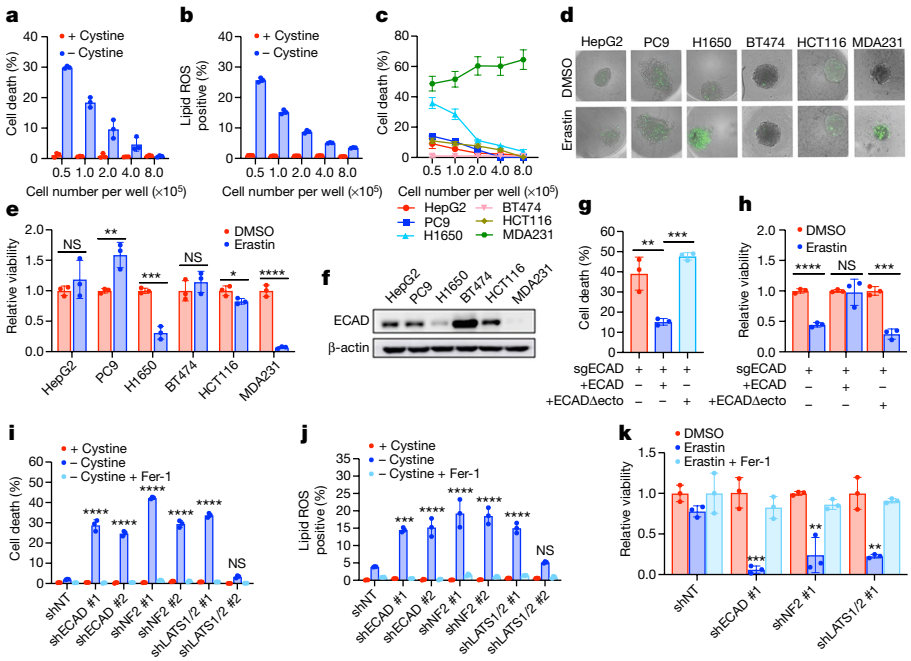

Fig. 1 | E-cadherin and the Hippo pathway regulate ferroptosis in a manner dependent on cell density. a, **b**, HCT116 cells were seeded at the indicated density in 6-well plates and cultured for 24 h. **a**, Ferroptosis was measured after cystine starvation for 30 h, by SYTOX Green staining followed by flow cytometry. **b**, Production of lipid reactive oxygen species (ROS) was measured and quantified after cystine starvation for 24 h, by staining of C11-BODIPY followed by flow cytometry. **c**, Ferroptosis was measured in the 6 indicated cell lines after cystine starvation for 30 h. **d**, **e**, Spheroids generated from the indicated cell lines were cultured for 72 h and treated with 15 μM erastin for 30 h. Dead cells were stained by SYTOX Green (**d**) (original magnification, ×40) and cell viability was assayed by measuring cellular ATP levels (**e**). NS, not significant ($P = 0.3757$, 0.3572; from left to right). $^{*}P = 0.0323$, $^{**}P = 0.0086$, $^{***}P = 0.0004$, $^{****}P < 0.0001$; two-tailed *t*-test. **f**, Western blot of ECAD levels in the indicated cell lines. Image represents three experiments; see Supplementary Fig. 1 for raw blots. **g**, Ferroptosis after cystine starvation for 30 h in HCT116 cells depleted of ECAD using single-guide RNA (sgECAD) and in ECAD-depleted cells expressing full-length or ectodomain-truncated (Δecto) ECAD. $^{**}P = 0.0025$, $^{***}P = 0.0005$; one-way analysis of variance (ANOVA). **h**, Viability of spheroids generated from cells as in **g** after treatment with erastin or dimethylsulfoxide (DMSO) control. NS, $P = 0.8683$. $^{***}P = 0.0004$, $^{****}P < 0.0001$; two-tailed *t*-test. **i**, Ferroptosis of HCT116 cells after cystine starvation for 30 h and the addition of 2 μM ferrostatin-1 (Fer-1). NS, $P = 0.6880$. $^{****}P < 0.0001$; one-way ANOVA. Note that shLATS1/2 #2 did not knockdown LATS2 (Extended Data Fig. 3e) and thus did not sensitize cells to ferroptosis. **j**, Lipid ROS production of cells as in **i**. NS, $P = 0.9383$. $^{***}P = 0.0001$, $^{****}P < 0.0001$; one-way ANOVA. **k**, Viability of spheroids generated from HCT116 cells after the indicated treatments. $^{**}P = 0.0012$, 0.0010 (left to right), $^{***}P = 0.0002$; one-way ANOVA. All data are mean ± s.d. from $n = 3$ biological replicates.

the transcriptional activity of YAP (also known as YY1AP1) with its primary binding partners, the TEAD family of transcription factors[22]. Low cell density, loss of ECAD or *NF2* RNAi all increased YAP activity and upregulated transcription of the canonical YAP targets *CTGF* and *CYR61* (Extended Data Fig. 3h–l). Knockdown of *ECAD*, *NF2*, *LATS1* and *LATS2* all sensitized HCT116 cells to ferroptosis in cell culture and spheroids (Fig. 1i–k and Extended Data Fig. 4a–c). Notably, knockdown of *ECAD*, *NF2*, *LATS1* and *LATS2* did not decrease cell proliferation within the time frame of the experiment, ruling out the possibility that increased ferroptosis was due to reduced cell confluence (Extended Data Fig. 4d). In addition, p21-activated kinase (PAK) can phosphorylate and inactivate NF2[17]. Consistently, constitutively active PAK (PAK-CAAX), but not its inactive mutant form (PAK-CAAX(K290R)), enhanced YAP activity and ferroptosis (Extended Data Fig. 4e–h). Together, ECAD and Hippo signalling negatively regulate ferroptosis.

Heterozygous deletion and loss-of-function mutations of the *NF2* gene are detected with high frequency in malignant mesothelioma, and inactivation of either NF2 or LATS1 or LATS2 is observed in approximately 50% of patients with malignant mesothelioma[10,11]. We assessed NF2 status and ferroptosis sensitivity in a cohort of human malignant mesothelioma cell lines. Of ten patient-derived cell lines we examined, four had wild-type NF2 expression, and six were NF2-defective[21] (Fig. 2a). All NF2 wild-type cells expressed a cadherin protein (not necessarily ECAD) and either LATS1 or LATS2 (Fig. 2a and Extended Data Fig. 5a). Several NF2-mutant cell lines can undergo potent ferroptosis even at the highest tested density and in spheroids, whereas all NF2 wild-type cells were relatively insensitive to ferroptosis under the same conditions (Fig. 2b, c and Extended Data Fig. 5b). Consistently, *NF2* RNAi sensitized confluent NF2 wild-type 211H cells to ferroptosis (Fig. 2d, e and Extended Data Fig. 5c, d), and NF2 reconstitution in confluent, NF2-defective Meso33 cells decreased nuclear localization of YAP and mitigated ferroptosis (Extended Data Fig. 5e–h). Furthermore, we generated a doxycycline (Dox)-inducible system to express NF2 in Meso33 cells (Fig. 2f). Indeed, Dox-induced restoration of NF2 inhibited ferroptosis at high density and in a spheroid model (Fig. 2g, h and Extended Data Fig. 5i).

Of the NF2 wild-type mesothelioma cells tested, only H-meso cells expressed ECAD (Fig. 2a). 211H cells express NCAD in a manner dependent on cell density (Extended Data Fig. 6a). We found that NCAD was similarly able to suppress ferroptosis in these cells and signal through the NF2–YAP axis (Extended Data Fig. 6b–k). We also observed cell-density-dependent, NF2-regulated ferroptosis in MEFs, which are not of epithelial origin (Extended Data Fig. 7a–k). Notably, we also observed a modest effect of cell density in a Burkitt lymphoma cell line, which does not express YAP or its homologue TAZ (Extended Data Fig. 7l–m), suggesting an alternative mechanism (cystine production by transsulfuration could be a contributor, as previously reported[23]).

The correlation between YAP activity and ECAD- or NF2-regulated ferroptosis prompted us to perform additional functional experiments to determine whether YAP promotes ferroptosis. The YAP(S127A) mutant cannot be phosphorylated by LATS1 or LATS2 at the Ser127 residue, thus enhancing nuclear retention and transcriptional

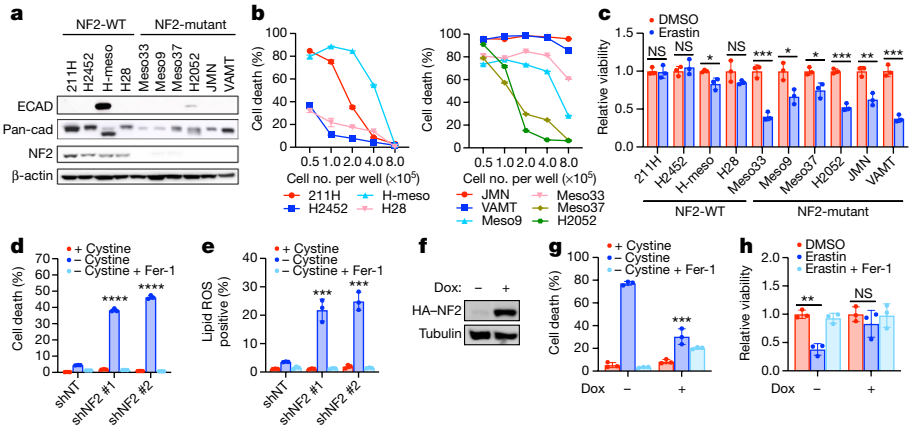

Fig. 2 | NF2 mediates cell-density-dependent inhibition of ferroptosis in mesothelioma cells. a, Western blot analysis of the expression of ECAD, pan-cadherin (pan-cad) and NF2 in a panel of mesothelioma cell lines cultured at high confluence. **b**, NF2 wild-type (WT; left) or mutant (right) mesothelioma cells were seeded at the indicated densities, and cell death was measured after cystine starvation for 24 h. **c**, Spheroids generated from the indicated cell lines were treated with 10 μM erastin for 24 h before the measurement of cell viability by ATP levels. NS, $P = 0.8860$, 0.4981, 0.1474 (left to right). $^{*}P = 0.0203$, 0.0180, 0.0162 (left to right), $^{**}P = 0.0033$, $^{***}P = 0.0005$, 0.0001, 0.0003 (left to right); two-tailed *t*-test. **d**, Cell death was measured in confluent cells after cystine starvation for 24 h, with or without the addition of 2 μM Fer-1. $^{****}P < 0.0001$; one-way ANOVA. **e**, Lipid ROS production of cells as in **d** after 18 h of treatment. $^{***}P = 0.0005$, 0.0002 (left to right); one-way ANOVA. **f**, Western blot analysis confirming expression of NF2 in Meso33 cells containing Dox-inducible NF2 after 48 h of treatment with 1 μg ml^{-1} Dox. HA, haemagglutinin tag. **g**, Cells in the presence or absence of Dox after cystine starvation for 12 h. $^{***}P = 0.0003$; two-tailed *t*-test. **h**, Spheroids were grown in the presence or absence of Dox for 72 h, at which point 10 μM erastin was added. Cell viability was measured by ATP levels after 24 h. NS, $P = 0.3393$. $^{**}P = 0.0010$; two-tailed *t*-test. All data are mean ± s.d. from $n = 3$ biological replicates.

regulatory activity even at high density[20,24,25] (Extended Data Fig. 8a–d). HCT116 or 211H cells that express YAP(S127A) were markedly more sensitive to ferroptosis at high density or in spheroids (Fig. 3a–c and Extended Data Fig. 8e–k). HCT116 cells that lack YAP were no longer sensitized to ferroptosis after *NF2* RNAi (Fig. 3d and Extended Data Fig. 8l), demonstrating that NF2 suppresses ferroptosis by inhibiting YAP activity.

Subsequently, we examined a range of putative YAP and TEAD gene targets that are known regulators of ferroptosis. Putative YAP–TEAD gene targets were selected from the TEAD4 ENCODE chromatin immunoprecipitation followed by high-throughput sequencing (ChIP–seq) datasets GSM1010875 and GSM1010868. Among these genes, we found that transferrin receptor 1 (*TFRC*) and acyl-CoA synthetase long chain family member 4 (*ACSL4*)—both crucial mediators of ferroptosis[14,26]—are genuine targets of the YAP–TEAD complex. Expression of TFRC and ACSL4 decreased with increasing cell density, and TFRC and ACSL4 were both upregulated by depletion of ECAD, knockdown of NF2 or overexpression of YAP(S127A) (Fig. 3e–h). TEAD4 binds

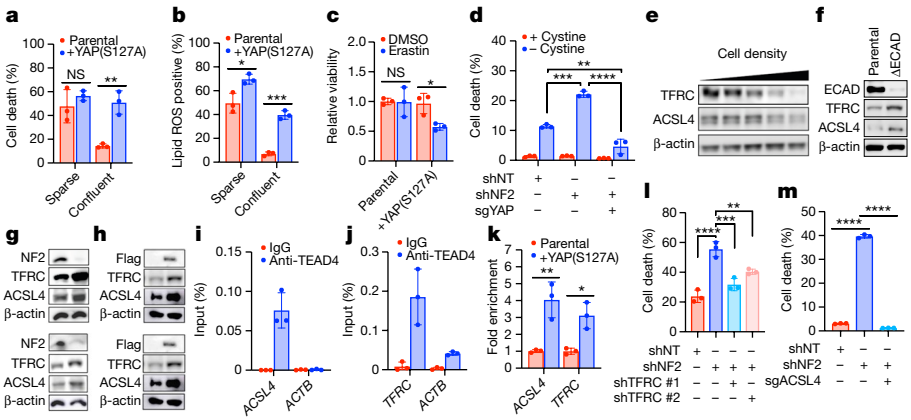

Fig. 3 | The transcriptional regulatory activity of YAP promotes ferroptosis. a, Cells were cultured as indicated. Cell death was measured after cystine starvation for 24 h. NS, $P = 0.3525$. $^{**}P = 0.0031$; two-tailed *t*-test. **b**, Lipid ROS production of cells after cystine starvation for 16 h. $^{*}P = 0.0202$, $^{***}P = 0.0001$; two-tailed *t*-test. **c**, Spheroids generated from parental HCT116 cells and YAP(S127A)-overexpressing cells were treated with erastin or DMSO as indicated, and cell viability was measured by cellular ATP levels. NS, $P = 0.957$. $^{*}P = 0.0200$; two-tailed *t*-test. **d**, Ferroptosis of the indicated cells after cystine starvation for 24 h and transfection with non-targeting shRNA (shNT), *NF2* shRNA (shNF2) or CRISPR–Cas9-mediated knockout of *YAP* (sgYAP). $^{**}P = 0.0043$, $^{***}P = 0.0004$, $^{****}P < 0.0001$; one-way ANOVA. **e**, Western blot analysis of TFRC and ACSL4 in 211H cells seeded at increasing density. **f**, Western blot analysis of TFRC and ACSL4 in parental and ECAD-depleted (ΔECAD) HCT116 cells. **g**, **h**, Western blot analysis of TFRC and ACSL4 in HCT116 (top) or 211H (bottom) cells transfected with shNT or shNF2 (**g**) or overexpressing YAP(S127A) (**h**). **i**, ChIP analysis of TEAD4 binding to the *ACSL4* promoter in 211H cells using control immunoglobulin G (IgG) or an anti-TEAD4 antibody. Values are percentage of input. Quantitative PCR (qPCR) primers were designed based on TEAD4-binding peak regions depicted in the ENCODE TEAD4 ChIP–seq datasets. **j**, TEAD4 binding to the promoter region of *TFRC* was analysed as described in **i**. **k**, ChIP analysis monitoring the occupancy of TEAD4 on the *ACSL4* and *TFRC* promoters in parental or YAP(S127A)-overexpressing 211H cells. Enrichment was calculated based on qPCR relative to the IgG control. $^{*}P = 0.0103$, $^{**}P = 0.0079$; two-tailed *t*-test. **l**, Cell death was measured in HCT116 cells expressing the indicated shRNAs after cystine starvation for 30 h. $^{**}P = 0.0072$, $^{***}P = 0.0004$, $^{****}P < 0.0001$; one-way ANOVA. **m**, Cell death was measured in HCT116 cells expressing indicated shRNA and/or sgRNA, after cystine starvation for 30 h. $^{****}P < 0.0001$; one-way ANOVA. All data are mean ± s.d. from $n = 3$ biological replicates.

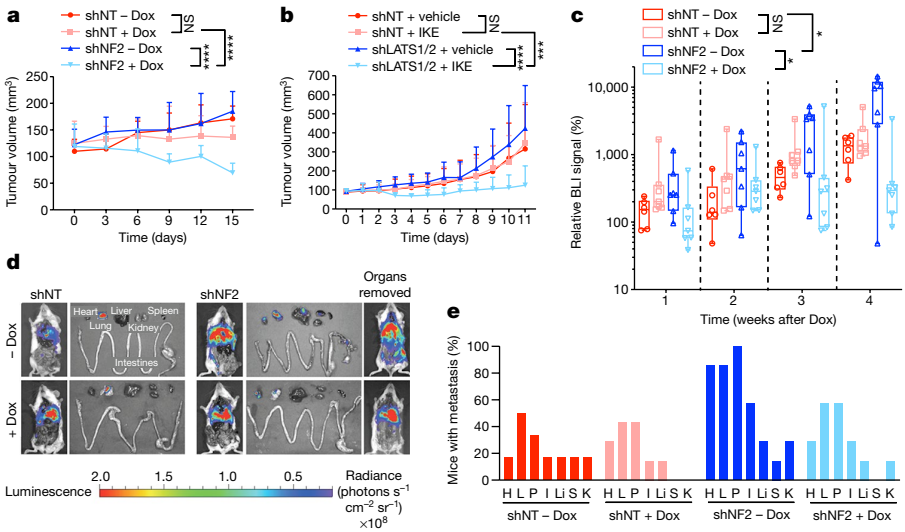

Fig. 4 | NF2 dictates GPX4 dependency in mouse models of mesothelioma. a, Growth curves of tumours derived from GPX4-knockout (GPX4-iKO) 211H cells containing shNF2 or shNT injected subcutaneously into nude mice fed Dox or a normal diet ($n = 8$ per group). NS, $P = 0.6776$. ****$P < 0.0001$; two-way ANOVA. **b**, The indicated HCT116 cells were injected subcutaneously into nude mice ($n = 6$ per group). Tumours were grown to a volume of 90 mm^3, at which point 50 mg kg^{-1} IKE was administered intraperitoneally daily for 12 days. NS, $P = 0.9808$. ***$P = 0.0001$, ****$P < 0.0001$; two-way ANOVA. For knockdown efficiency of LATS1 and LATS2, see Extended Data Fig. 3e. **c**, shNT-GPX4-iKO or shNF2-GPX4-iKO 211H cells were orthotopically injected into the pleural cavity of mice. The percentage change in the relative bioluminescent imaging (BLI) signal (photons s^{-1}) versus time-point 0 is shown. $n = 6$ (shNT − Dox) or 7 mice for each group. Box plots represent median ± interquartile range, whiskers represent the range of values. NS, $P = 0.1545$. *$P = 0.0237$, 0.0287 (top to bottom); two-way ANOVA. **d**, Bioluminescence imaging in excised organs, and in mouse bodies before and after organs were removed. **e**, Percentage of mice in each group with metastases in excised organs. shNT − Dox: $n = 6$; shNT + Dox, shNF2 − Dox, shNF2 − Dox: $n = 7$. H, heart; I, intestines/mesenteric lymph nodes; K, kidneys L, lung; Li, liver; P, peritoneum; S, spleen. Data in **a** and **b** are mean ± s.d.

to the promoter regions of *TFRC* and *ACSL4* genes, and binding was enhanced by overexpression of YAP(S127A) (Fig. 3i–k). Confluent HCT116 cells were sensitized to ferroptosis after the expression of either TFRC or ACSL4, and co-expression of both further enhanced cell death (Extended Data Fig. 8m, n). Conversely, reduced expression of TFRC or ACSL4 mitigated ferroptosis in sensitized cells (Fig. 3l, m and Extended Data Fig. 8o–r). Together, these data indicate that upregulation of TFRC and ACSL4 contributes to the ability of YAP to promote ferroptosis. Notably, co-overexpression of TFRC and ACSL4 did not restore ferroptosis in confluent cells to the level of that in sparse cells, even when the ectopic ACSL4 level was higher than that in sparse cells (Extended Data Fig. 8m, n), which suggests that additional YAP target genes contribute to this process.

As loss of NF2 frequently drives mesothelioma[10,11], we examined whether NF2 status could predict mesothelioma sensitivity to ferroptosis. We generated Dox-inducible, CRISPR–Cas9-mediated GPX4-knockout (GPX4-iKO) 211H cells containing short hairpin RNA (shRNA) against *NF2* (shNF2) or non-targeting shRNA (shNT) (Extended Data Fig. 9a). Spheroids cultured after *NF2* shRNA cells were more sensitive than shNT cells to GPX4 knockout-induced ferroptosis (Extended Data Fig. 9b). We then used shNT-GPX4-iKO cells and shNF2-GPX4-iKO cells to produce subcutaneous xenograft tumours in athymic nude mice. In tumours, knockdown of NF2 increased the expression of TFRC, ACSL4 and nuclear YAP (Extended Data Fig. 9c). The addition of Dox sharply reduced the expression of GPX4 in tumours; in *NF2* RNAi tumours, Dox addition resulted in increased expression of the ferroptosis marker PTGS2[3] and reduced proliferation, as measured by Ki67 staining (Extended Data Fig. 9d). Notably, after Dox addition, shNF2 tumours receded whereas shNT tumours only showed a decrease in growth (Fig. 4a and Extended Data Fig. 9e). Similarly, knockdown of LATS1 and LATS2 rendered xenograft tumours generated by HCT116 cells significantly more sensitive to imidazole ketone erastin (IKE), an erastin derivative amenable for use in vivo[27] (Fig. 4b and Extended Data Fig. 9f).

We next developed an intrapleural mouse model of mesothelioma, by orthotopically implanting shNF2-GPX4-iKO or shNT-GPX4-iKO cells containing a retroviral TK-GFP-luciferase (TGL) reporter. shNF2-GPX4-iKO cells grew more aggressively than shNT-GPX4-iKO cells in mice, consistent with the tumour-suppressive nature of NF2; the addition of Dox reduced the growth of shNF2 tumours, whereas shNT tumours were unaffected (Fig. 4c and Extended Data Fig. 9g). After euthanization, various organs were excised for bioluminescence imaging. shNT tumours grew within the pleural cavity, attaching to the aortic arch, lung or thoracic muscles, whereas shNF2 tumours metastasized to the pericardium, peritoneum, abdominal organs including liver, intestine and distal lymph nodes (Fig. 4d, e)—consistent with previous reports that NF2 loss enhances metastasis of mesothelioma[10]. Supporting this notion, spheroids cultured from *NF2* shRNA cells extended more finger-like protrusions into Matrigel (Extended Data Fig. 9h). Importantly, the metastatic capability of *NF2* shRNA tumours was reduced by Dox-induced knockout of GPX4 (Fig. 4d, e). Therefore, NF2 status might be useful as a biomarker to predict mesothelioma metastasis and responsiveness to the induction of ferroptotic cell death.

Sorafenib, an orally administered multi-kinase inhibitor used for the treatment of hepatocellular carcinoma and renal cell carcinoma, also induces ferroptosis by inhibition of the x_c^- amino acid antiporter[28]. The potential for sorafenib as a therapy for malignant mesothelioma has been tested in clinical trials. The results suggest that sorafenib can stabilize the disease but achieves responses in only a small proportion of unselected patients[29,30]. However, these trials did not examine the genetic status of the NF2–Hippo pathway. We found that sorafenib induced ferroptosis in a manner that is dependent on cell density and Hippo signalling (Extended Data Fig. 10a–g). In addition, in epithelial cancer cells, decreased levels of ECAD, NF2 or Hippo pathway activity, and enhanced activation of YAP can promote epithelial–mesenchymal transition (EMT) and metastasis[19]. Consistently, as TGFβ can induce the expression of several EMT genes, it also enhanced ferroptosis in mammary tumour cells isolated from MMTV-neu mice at high cell density (Extended Data Fig. 10h–j).

Collectively, we describe a non-cell-autonomous mechanism for the regulation of ferroptosis: neighbouring cells can have a considerable effect on the decision-making of ferroptosis via the

cadherin–NF2–Hippo–YAP signalling axis. Considering that multicellular organisms are under frequent insult of oxidative stress, this intercellular mechanism might represent another layer of crucial defence to protect themselves from ferroptosis, a terminal consequence of oxidative stress.

Because cellular metabolism has a crucial role in ferroptosis, and enhanced proliferation often leads to stronger metabolism, it is possible that proliferation-stimulating oncogenic mutation may be a good predictor of ferroptosis sensitivity. However, previous publications argue against this view. For example, loss of function of the tumour suppressors p53 and BAP1 increases resistance, instead of sensitivity, to ferroptosis[5,7]. Furthermore, unlike YAP(S127A), overexpression of the oncogenic PIK3CA(H1047R) mutant did not sensitize confluent 211H cells to ferroptosis, although both increased proliferation (Extended Data Fig. 10k–m). Together, oncogenic mutations may affect ferroptosis by mechanisms other than enhancing proliferation.

As the cadherin–NF2–Hippo–YAP signalling axis is frequently mutated in cancer, this study has clear implications for cancer therapies—malignant alterations of several components in this signalling axis all sensitize cancer cells to ferroptosis. A potential concern about the feasibility of ferroptosis-inducing cancer therapy is whether there is any selectivity of the ferroptosis-inducing agents towards cancer cells compared with normal tissue. Our finding suggests that there might be a dose-responsive window for cancers that contain certain genetic signatures and that ferroptosis-inducing cancer therapies—if available (IKE and sorafenib hold potential for this purpose)—might have considerable benefits in overcoming cancer resistance to current treatments.

Online content

Any methods, additional references, Nature Research reporting summaries, source data, statements of data availability and associated accession codes are available at https://doi.org/10.1038/s41586-019-1426-6.

Received: 7 November 2018; Accepted: 27 June 2019;
Published online: 24 July 2019

1. Stockwell, B. R. et al. Ferroptosis: a regulated cell death nexus linking metabolism, redox biology, and disease. *Cell* **171**, 273–285 (2017).
2. Gao, M. & Jiang, X. To eat or not to eat—the metabolic flavor of ferroptosis. *Curr. Opin. Cell Biol.* **51**, 58–64 (2018).
3. Yang, W. S. et al. Regulation of ferroptotic cancer cell death by GPX4. *Cell* **156**, 317–331 (2014).
4. Gao, M. et al. Role of mitochondria in ferroptosis. *Mol. Cell* **73**, 354–363.e3 (2019).
5. Jiang, L. et al. Ferroptosis as a p53-mediated activity during tumour suppression. *Nature* **520**, 57–62 (2015).
6. Jennis, M. et al. An African-specific polymorphism in the *TP53* gene impairs p53 tumor suppressor function in a mouse model. *Genes Dev.* **30**, 918–930 (2016).
7. Zhang, Y. et al. BAP1 links metabolic regulation of ferroptosis to tumour suppression. *Nat. Cell Biol.* **20**, 1181–1192 (2018).
8. Viswanathan, V. S. et al. Dependency of a therapy-resistant state of cancer cells on a lipid peroxidase pathway. *Nature* **547**, 453–457 (2017).
9. Hangauer, M. J. et al. Drug-tolerant persister cancer cells are vulnerable to GPX4 inhibition. *Nature* **551**, 247–250 (2017).
10. Hmeljak, J. et al. Integrative molecular characterization of malignant pleural mesothelioma. *Cancer Discov.* **8**, 1548–1565 (2018).
11. Bueno, R. et al. Comprehensive genomic analysis of malignant pleural mesothelioma identifies recurrent mutations, gene fusions and splicing alterations. *Nat. Genet.* **48**, 407–416 (2016).
12. Seiler, A. et al. Glutathione peroxidase 4 senses and translates oxidative stress into 12/15-lipoxygenase dependent- and AIF-mediated cell death. *Cell Metab.* **8**, 237–248 (2008).
13. Schneider, M. et al. Absence of glutathione peroxidase 4 affects tumor angiogenesis through increased 12/15-lipoxygenase activity. *Neoplasia* **12**, 254–263 (2010).
14. Gao, M., Monian, P., Quadri, N., Ramasamy, R. & Jiang, X. Glutaminolysis and transferrin regulate ferroptosis. *Mol. Cell* **59**, 298–308 (2015).
15. van Roy, F. & Berx, G. The cell–cell adhesion molecule E-cadherin. *Cell. Mol. Life Sci.* **65**, 3756–3788 (2008).
16. Kim, N. G., Koh, E., Chen, X. & Gumbiner, B. M. E-cadherin mediates contact inhibition of proliferation through Hippo signaling-pathway components. *Proc. Natl Acad. Sci. USA* **108**, 11930–11935 (2011).
17. Okada, T., Lopez-Lago, M. & Giancotti, F. G. Merlin/NF-2 mediates contact inhibition of growth by suppressing recruitment of Rac to the plasma membrane. *J. Cell Biol.* **171**, 361–371 (2005).
18. Zhao, B., Lei, Q. Y. & Guan, K. L. The Hippo–YAP pathway: new connections between regulation of n size and cancer. *Curr. Opin. Cell Biol.* **20**, 638–646 (2008).
19. Pan, D. The Hippo signaling pathway in development and cancer. *Dev. Cell* **19**, 491–505 (2010).
20. Li, W., Cooper, J., Karajannis, M. A. & Giancotti, F. G. Merlin: a tumour suppressor with functions at the cell cortex and in the nucleus. *EMBO Rep.* **13**, 204–215 (2012).
21. Li, W. et al. Merlin/NF2 loss-driven tumorigenesis linked to CRL4(DCAF1)-mediated inhibition of the hippo pathway kinases Lats1 and 2 in the nucleus. *Cancer Cell* **26**, 48–60 (2014).
22. Dupont, S. et al. Role of YAP/TAZ in mechanotransduction. *Nature* **474**, 179–183 (2011).
23. Falk, M. H. et al. Apoptosis in Burkitt lymphoma cells is prevented by promotion of cysteine uptake. *Int. J. Cancer* **75**, 620–625 (1998).
24. Varelas, X. & Wrana, J. L. Coordinating developmental signaling: novel roles for the Hippo pathway. *Trends Cell Biol.* **22**, 88–96 (2012).
25. Zhao, B. et al. Inactivation of YAP oncoprotein by the Hippo pathway is involved in cell contact inhibition and tissue growth control. *Genes Dev.* **21**, 2747–2761 (2007).
26. Doll, S. et al. ACSL4 dictates ferroptosis sensitivity by shaping cellular lipid composition. *Nat. Chem. Biol.* **13**, 91–98 (2017).
27. Zhang, Y. et al. Imidazole ketone erastin induces ferroptosis and slows tumor growth in a mouse lymphoma model. *Cell Chem. Biol.* **26**, 623–633.e9 (2019).
28. Dixon, S. J. et al. Pharmacological inhibition of cystine–glutamate exchange induces endoplasmic reticulum stress and ferroptosis. *eLife* **3**, e02523 (2014).
29. Dubey, S. et al. A phase II study of sorafenib in malignant mesothelioma: results of Cancer and Leukemia Group B 30307. *J. Thorac. Oncol.* **5**, 1655–1661 (2010).
30. Papa, S. et al. Phase 2 study of sorafenib in malignant mesothelioma previously treated with platinum-containing chemotherapy. *J. Thorac. Oncol.* **8**, 783–787 (2013).

METHODS

Cell culture. MEFs, mouse NF639 cells, human epithelial tumour cells, and human mesothelioma cells were cultured in DMEM containing 10% fetal calf serum (FCS), 2 mM L-glutamine, 100 U ml^{-1} penicillin and 100 $\mu g\ ml^{-1}$ streptomycin. CA-46 Burkitt lymphoma cells were cultured in RPMI medium supplemented with 20% serum and 100 U ml^{-1} penicillin and 100 $\mu g\ ml^{-1}$ streptomycin. The mesothelioma cell line panel was a gift from the Giancotti Laboratory. Media were prepared by the MSKCC Media Preparation Core Facility. All cell lines were subjected to STR authentication through ATCC and were tested for mycoplasma contamination.

Generation of 3D spheroids. Spheroids were generated by plating tumour cells at 10^3 per well into U-bottom Ultra Low Adherence (ULA) 96-well plates (Corning). Optimal 3D structures were achieved by centrifugation at 600*g* for 5 min followed by addition of 2.5% (v/v) Matrigel (Corning). Plates were incubated for 72 h at 37 °C, 5% CO_2, 95% humidity for formation of a single spheroid of cells. Spheroids were then treated with erastin in fresh medium containing Matrigel for the indicated time.

Induction and inhibition of ferroptosis. To induce ferroptosis, cells with different density were seeded in 6-well plates. For cystine-starvation experiments, cells were washed twice with PBS and then cultured in cystine-free medium in the presence of 10% (v/v) dialysed FBS for the indicated time. The ferroptosis-inducing compounds erastin and RSL3 and the ferroptosis inhibitor ferrostatin-1 were purchased from Sigma-Aldrich.

Measurement of cell death, cell viability and lipid peroxidation. Cell death was analysed by staining for propidium iodide (Invitrogen) or SYTOX Green (Invitrogen) followed by microscopy or flow cytometry. For 3D spheroids, cell viability was determined using the CellTiter-Glo 3D Cell Viability Assay (Promega) according to the manufacturer's instructions. Viability was calculated by normalizing ATP levels to spheroids treated with normal medium. To analyse lipid peroxidation, cells were stained 5 μM BODIPY-C11 (Invitrogen) for 30 min at 37 °C followed by flow cytometric analysis. Lipid ROS-positive cells are defined as cells with FITC fluorescence greater than 99% of the unstained sample.

Immunoblotting. Nuclear and non-nuclear (membranes and cytosol) fractions were prepared as previously described. Proteins in the cell lysate were resolved on 8% or 15% SDS–PAGE gels and transferred to a nitrocellulose membrane. Membranes were incubated in 5% skim milk for 1 h at room temperature and then with primary antibodies diluted in blocking buffer at 4 °C overnight. The following primary antibodies were used: rabbit anti-GPX4, mouse anti E-cadherin, rabbit anti-N-cadherin, rabbit anti-NF2/Merlin, rabbit anti-transferrin receptor (Abcam, Cambridge), mouse anti-β-actin, mouse anti-Flag, mouse anti-HA (Sigma-Aldrich), rabbit anti-NF2/Merlin, rabbit anti-phospho-NF2/Merlin (Ser518), rabbit anti-LATS1, rabbit anti-LATS2, rabbit anti-YAP, rabbit anti-phospho-YAP (Ser127), mouse anti-CAS9, rabbit anti-p110α, mouse anti-AKT, rabbit anti-phospho-AKT (Ser473), rabbit anti-TAZ, rabbit anti-pan cadherin (Cell Signaling), rabbit anti-ACSL4 (Thermo Fisher), mouse anti-α-tubulin (Calbiochem), rabbit anti-GFP (Invitrogen). Goat anti-mouse or donkey anti-rabbit IgG (Invitrogen) conjugated to horseradish peroxidase (HRP) and an Amersham Imager 600 (GE Healthcare Life Sciences) was used for detection. Representative blots of at least two independent experiments are shown. After three washes, the membranes were incubated with goat anti-mouse HRP-conjugated antibody or donkey anti-rabbit HRP-conjugated antibody at room temperature for 1 h and subjected to chemiluminescence using Clarity Western ECL Substrate (Bio-Rad).

Plasmids and cloning. pWZL Blast mouse E-cadherin and pWZL Blast DN E-cadherin were from the Weinberg Laboratory (Addgene plasmids 18804 and 18800, respectively). pRK5-Flag-HA-NF2 was from the Giancotti laboratory (Addgene plasmid 27104). The 8xGTIIC-luciferase reporter was from the Piccolo laboratory (Addgene plasmid 34615). mCherry-TFR-20 was from the Davidson laboratory (Addgene plasmid 55144). pQCXIH-Flag-YAP-S127A was from the Guan laboratory (Addgene plasmid 33092). pBABE-Flag-HA-NF2 was generated by PCR from pRK5-Flag-HA-NF2 (primers listed in Supplementary Table 2), digested by PacI and EcoRI FastDigest restriction enzymes (Thermo Fisher), and ligated into the empty pBABE-puro backbone using T4 ligase (NEB). FUW-tetO-Flag-HA-NF2 was created by digesting pRK5-Flag-HA-NF2 with EcoRI and XbaI and was ligated into the FUW-tetO-MCS vector from the Piccolo laboratory (Addgene plasmid 84008). FUW-m2rtTA was from the Jaenisch laboratory (Addgene plasmid 20342). PIK3CA(H1047R) was a gift from the Cantley laboratory (Weill Cornell Medicine).

Gene silencing and expression. Lentiviral vectors encoding shRNAs targeting human *ECAD*, human *NCAD*, human and mouse *Nf2*, human *LATS1* and *LATS2*, and human *TFRC* were generated by the core facility of MSKCC and are listed in Supplementary Table 1. Lentiviruses were produced by the co-transfection of the lentiviral vector with the Delta-VPR envelope and CMV VSV-G packaging plasmids into 293T cells using PEI. Medium was changed 12 h after transfection. The supernatant was collected 48 h after transfection and passed through a 0.45-μm filter to eliminate cells. Cells were incubated with infectious particles in the presence of 4 $\mu g\ ml^{-1}$ polybrene (Sigma-Aldrich) overnight and cells were given fresh complete medium. After 48 h, cells were placed under the appropriate antibiotic selection.

Generation of constitutive and inducible CRISPR–Cas9-mediated gene knockouts. ECAD, YAP- and ACSL4-depleted cells were generated using the CRISPR–Cas9-mediated knockout system. HCT116 cells were transfected with a human *ECAD* CRISPR–Cas9 knockout plasmid (sc-400031), and HCT116-shNF2 cells were transfected with a human *YAP* CRISPR–Cas9 knockout plasmid (sc-400040) or a human *ACSL4* CRISPR–Cas9 KO plasmid (sc-401649), all purchased from Santa Cruz Biotechnology. The target sequence was a pool of three different gRNA plasmids located within the coding DNA sequence fused to *Streptococcus pyogenes Cas9* and GFP. Single GFP^+ cells were sorted using a BD FACSAria II cytometer (BD Biosciences) and a 96-well plate, and single-cell clones were tested by western blotting.

The lentiviral Dox-inducible Flag–Cas9 vector pCW-Cas9 and pLX-sgRNA were from E. Lander and D. Sabatini (Addgene plasmids 50661 and 50662, respectively). Guide RNA sequence CACGCCCGATACGCTGAGTG was used to target human *GPX4*. To construct the lentiviral sgRNA vector for *GPX4*, a pair of oligonucleotides (forward and reverse) was annealed, phosphorylated and ligated into pLX-sgRNA. Lentiviral particles containing the sgRNA or Cas9 vectors were produced by co-transfection of the vectors with the Delta-VPR envelope and CMV VSV-G packaging plasmids into 293T cells using PEI. Medium was changed 12 h after transfection and supernatant was collected 48 h after transfection. MSTO-211H cells in 6-well tissue culture plates were infected in pCW-Cas9 virus-containing supernatant containing 4 $\mu g\ ml^{-1}$ of polybrene. Twenty-four hours after infection, virus was removed, and cells were selected with 2 $\mu g\ ml^{-1}$ puromycin. Single clones were screened for inducible Cas9 expression. Dox (2 $\mu g\ ml^{-1}$) was added to the culture medium for 3 days. Single clones with Cas9 expression were infected with *GPX4* gRNA virus-containing supernatant containing 8 $\mu g\ ml^{-1}$ polybrene. Twenty-four hours after infection, virus was removed and cells were selected with 10 $\mu g\ ml^{-1}$ blasticidin. Single clones with Dox-inducible Cas9 expression and *GPX4* knockout were amplified for further experiments, named GPX4-iKO MSTO-211H cells.

ChIP assay. Cells were crosslinked in 0.75% formaldehyde for 15 min, and glycine was added to a final concentration of 125 mM for 5 min. After washing with cold PBS, cells were collected in PBS and sonicated on an ultrasonic homogenizer for 10 min at 20% power on ice to shear DNA to an average fragment size of 200–1,000 bp. Fifty microlitres of each sonicated sample was removed to determine the DNA concentration and fragment size. Cell lysates were incubated overnight with 20 μl Magna ChIP Protein A+G Magnetic Beads (EMD Millipore) and 10 μg ChIP grade TEAD4 antibody (Abcam) at 4 °C. Beads were collected, washed and treated with proteinase K for 2 h at 60 °C and RNase for 1 h at 37 °C. DNA was purified with a PCR purification kit (Qiagen). DNA fragments were assessed by quantitative PCR with reverse transcription (qRT–PCR) using the primer sequences listed in Supplementary Table 2. Samples were normalized to input DNA.

RNA extraction and qRT–PCR. RNA was extracted using the TRIzol reagent (Invitrogen). Samples were treated with chloroform (20%), vortexed briefly, and incubated at room temperature for 15 min. Samples were then centrifuged at high speed at 4 °C for 15 min. The aqueous phase was moved to a new tube and an equal volume of isopropanol was added. Samples were incubated at room temperature for 10 min, followed by centrifugation at high speed at 4 °C for 10 min. Pellets were washed in 95% ethanol, dried and resuspended in nuclease-free water. cDNA was synthesized using iScript cDNA Synthesis Kit according to the manufacturer's instructions (Bio-Rad). qRT–PCR was performed with IQ SYBR Green Supermix (Bio-Rad) in a CFX Connect Real-Time PCR Detection System (Bio-Rad). Primer sequences are listed in Supplementary Table 2.

In vivo xenograft mouse study. GPX4-iKO MSTO-211H cells were infected with lentiviral vectors encoding shRNAs targeting human *NF2* or non-targeting control (shNT) (GeneCopoeia). The resulting cells were called 'shNT-GPX4-iKO' and 'shNF2-GPX4-iKO' MSTO-211H cells. Six- to eight-week-old female athymic *nu/nu* mice were purchased from Envigo. For subcutaneous tumour models, mice were injected in the right flank with 1×10^7 shNT-GPX4-iKO or shNF2-GPX4-iKO MSTO-211H cells suspended in 150 μl Matrigel. Tumours were measured with callipers every three days. When tumours reached a mean volume of 100 mm^3, mice with similarly sized tumours were grouped into four treatment groups. For control or knockout cohorts, mice were given intraperitoneal injections of 0.9% sterile saline or Dox (100 mg kg^{-1} body weight) for two days. At the same time, mice were provided with either a normal or a Dox diet for control or knockout cohorts, respectively. For all experiments, mice were killed at a pre-determined endpoint. According to the Institutional Animal Care and Use Committee (IACUC) protocol for these experiments, once any tumour exceeded a volume of 1,000 mm^3, 1.5 cm in diameter or 10% of body weight, the mice would immediately be euthanized. At the end of the study, mice were euthanized with CO_2 and tumours were taken for immunohistochemical staining. Results are presented as mean tumour volume ± s.d.

For shLATS1/2 subcutaneous tumour models, female athymic *nu/nu* mice aged 6–8 weeks were injected in the right flank with 2×10^6 shNT HCT116 cells or shLATS1/2 HCT116 cells. Tumours were measured with callipers daily. When tumours reached a mean volume of 90 mm^3, mice were randomized into 4 groups and treated with vehicle (65% D5W (5% dextrose in water), 5% Tween-80, 30% PEG-400) or 50 mg kg^{-1} IKE (65% D5W (5% dextrose in water), 5% Tween-80, 30% PEG-400) via intraperitoneal injection once a day. At the end of the study, mice were euthanized with CO_2 and tumours were taken for measurement of weight. According to the IACUC protocol for these experiments, once any tumour exceeded a volume of 1,000 mm^3, 1.5 cm in diameter or 10% of body weight, the mice would immediately be euthanized.

All protocols for mouse experiments were approved by the Memorial Sloan Kettering Cancer Center IACUC.

Orthotopic pleural mesothelioma mouse model. shNT-GPX4-iKO and shNF2-GPX4-iKO MSTO-211H cells were infected with retroviral TK-GFP-luciferase (TGL) reporter vector. To develop the orthotopic mouse model of pleural mesothelioma, female NOD/SCID mice (Envigo) aged 6–8 weeks were used. Mice were anaesthetized using inhaled isoflurane and oxygen. Intrapleural injection of 2×10^6 shNT-GPX4-iKO-TGL or shNF2-GPX4-iKO-TGL MSTO-211H cells in 100 μl of serum-free medium via a left thoracic incision was performed to establish the orthotopic mesothelioma tumour model. Tumour growth was monitored by weekly BLI for luciferase and mice were monitored daily for survival. NOD/SCID mice bearing tumours were anaesthetized using isoflurane and injected intraperitoneally with 50 mg kg^{-1} D-luciferin (Molecular Probes). BLI was measured with 18 filters (500–840 nm) in an IVIS Spectrum (PerkinElmer) 10 min after injection. During image acquisition, mice were maintained on isoflurane via nose cone. Bioluminescence images were acquired using an IVIS Spectrum. The BLI signal was reported as total flux (photons per second), which represents the average of ventral and dorsal flux. At the end-point of the study, the mice were injected with D-luciferase and euthanized 10 min later. Organs were exposed and the BLI signal was measured. After organs were excised, BLI images were taken again as described. Imaging analysis was performed using the Living Image software (Caliper Life Sciences) All protocols for mouse experiments were approved by the Memorial Sloan Kettering Cancer Center IACUC.

Immunohistochemistry. Formalin-fixed, paraffin-embedded specimens were collected, and a routine H&E slide was first evaluated. Immunohistochemical staining was done on 5-μm-thick paraffin-embedded sections using mouse anti-NF2/Merlin (Abcam), rabbit anti-GPX4 (Abcam), rabbit anti-PTGS2 (Cell Signaling), mouse anti-Ki67 (Cell Signaling), rabbit anti-ACSL4 (Thermo Fisher), rabbit anti-TFRC (Abcam) and rabbit anti-YAP (Cell Signaling) antibodies with a standard avidin-biotin HRP detection system according to manufacturer's instructions (anti-mouse/rabbit HRP-DAB Cell & Tissue Staining Kit, R&D Systems). Tissues were counterstained with haematoxylin, dehydrated and mounted. In all cases, antigen retrieval was done with the BD Retrievagen Antigen Retrieval Systems as per manufacturer's instructions.

Tumour spheroid invasion assay. Spheroids were generated as described in 200 μl complete growth medium and cultured for 72 h after cell seeding. The ULA 96-well plates containing 3-day-old spheroids were placed on ice. One-hundred microlitres per well of growth medium was removed from the spheroid plates. Using ice-cold tips, 100 μl of Matrigel was transferred to each well and mixed gently with medium, avoiding disturbance of the spheroids. Plates were placed in an incubator at 37 °C to allow the Matrigel to solidify. One hour later, 100 μl per well of complete growth medium was added. Images for each tumour spheroid were taken 48 h later.

Statistical analysis. All statistical analyses were performed using GraphPad Prism 6.0 Software. Data are presented as mean ± s.d. from three independent experiments. *P* values were determined by Student's two-tailed *t*-test, one-way ANOVA or two-way ANOVA as indicated in the figure legends. For ANOVA, adjustments were made for multiple comparisons by Dunnett or Tukey corrections as appropriate. Exact *P* values can be found in figure legends. In cases where more than one comparison has the same statistical range, values are listed as they appear from left to right in the corresponding panel. No statistical methods were used to predetermine sample size. Unless stated otherwise, the experiments were not randomized and investigators were not blinded to allocation during experiments and outcome assessment.

Reporting summary. Further information on research design is available in the Nature Research Reporting Summary linked to this paper.

Data availability

For western blot source data, see Supplementary Fig. 1. For the gating strategy used for flow cytometry experiments, see Supplementary Fig. 2. Raw data for all experiments are available as Source Data to the relevant figures. ChIP–seq datasets analysed in this article are publicly available in the ENCODE database under the identifiers GSM1010875 and GSM1010868.

Acknowledgements We thank E. De Stanchina and E. Peguero for their help with mouse modelling experiments. We thank members of the Jiang laboratory for critical reading and suggestions. This work is supported by the National Institutes of Health (NIH) R01CA204232 (to X.J.), a Geoffrey Beene Cancer Research fund (to X.J.), a Functional Genomic Initiative fund (to X.J.), a China Scholarship Council fellowship (to J.W.), and NIH T32 fellowship 5T32GM008539-23 (to A.M.M.), National Cancer Institute R35CA209896 and P01CA087497 (to B.R.S.), National Natural Science Foundation of China 31871388 (to M.G.). This work is also supported by NCI cancer centre core grant P30 CA008748 to Memorial Sloan Kettering Cancer Center.

Author contributions J.W., A.M.M. and X.J. conceived the original idea and designed the study. J.W. and A.M.M. performed most experiments. M.G., H.B. and Y.L. generated several reagents and the inducible GPX4 knockout (GPX4-iKO) used in mouse experiments. B.R.S. supplied IKE and protocols for IKE administration to mice. Z.-N.C. and X.J. supervised the research. J.W., A.M.M., Z.-N.C. and X.J. wrote the paper.

Competing interests B.R.S. holds equity in and serves as a consultant to Inzen Therapeutics, consults with GLG and Guidepoint Global, and is an inventor on patents and patent applications related to IKE and ferroptosis.

Additional information

Supplementary information is available for this paper at https://doi.org/10.1038/s41586-019-1426-6.

Correspondence and requests for materials should be addressed to Z.-N.C. or X.J.

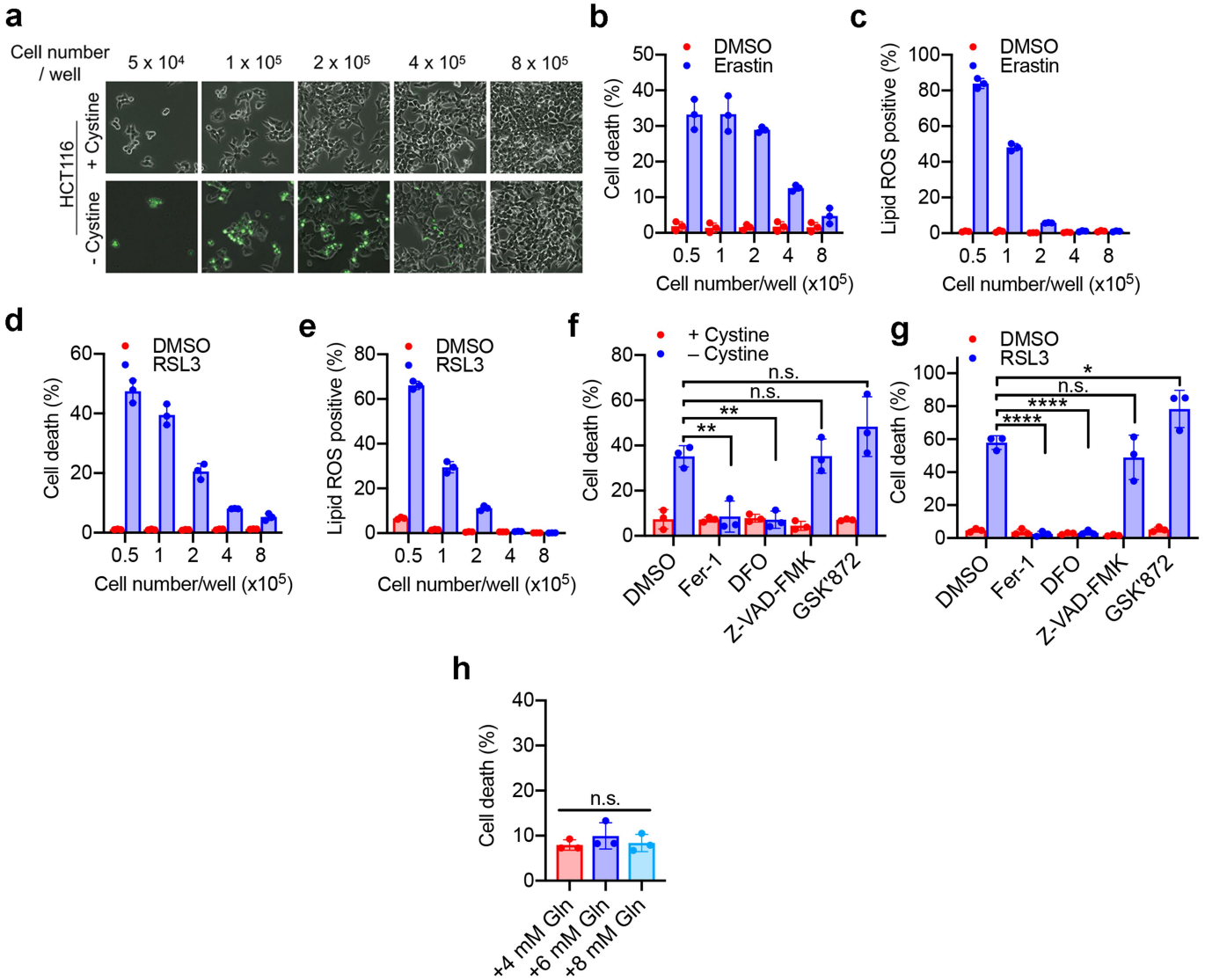

Extended Data Fig. 1 | Intercellular contact suppresses ferroptosis. **a**, **b**, HCT116 cells were seeded at the indicated density in 6-well plates and cultured for 24 h. **a**, Ferroptosis was measured by SYTOX Green staining after cystine starvation for 30 h. Phase contrast and fluorescent images are overlaid (original magnification, ×100). **b**, Cell death was measured in HCT116 cells at different densities treated with 30 μM erastin for 30 h, quantified by SYTOX Green staining followed by flow cytometry. **c**, Lipid ROS production of cells in **b** was assessed by C11-BODIPY staining followed by flow cytometry after 24 h of erastin treatment **d**, Cell death was measured in HCT116 cells cultured at the indicated cell densities and treated with 5 μM RSL3 for 24 h. **e**, Lipid ROS production in HCT116 cells cultured at the indicated cell densities and treated with 5 μM RSL3 for 16 h. **f**, HCT116 cells were seeded at 5×10^4 cells per well, grown for 24 h, and treated with: 1 μM Fer-1; 50 μg ml^{-1} of the iron chelator deferoxamine (DFO); 20 μM of the pan-caspase inhibitor Z-VAD-FMK; or 10 μM of the RIPK3 inhibitor GSK'872, in complete medium or cysteine-free medium for 30 h, followed by cell death measurement. n.s., $P = 0.9999$, 0.1995 (left to right). $^{**}P = 0.0070$, 0.0050; one-way ANOVA. **g**, Cell death was measured in HCT116 cells seeded at 5×10^4 cells per well, grown for 24 h and treated with 5 μM RSL3 or DMSO and inhibitors as in **f** for 24 h. n.s., $P = 0.4989$. $^{*}P = 0.0366$, $^{****}P < 0.0001$; one-way ANOVA. **h**, Cell death analysis in HCT116 cells seeded at 8×10^5 cells per well, grown for 24 h and treated with cystine-free medium containing the indicated amounts of glutamine for 30 h. Cell death was measured by SYTOX Green staining followed by flow cytometry. n.s., $P = 0.5156$; one-way ANOVA. All data are mean ± s.d. from $n = 3$ biological replicates.

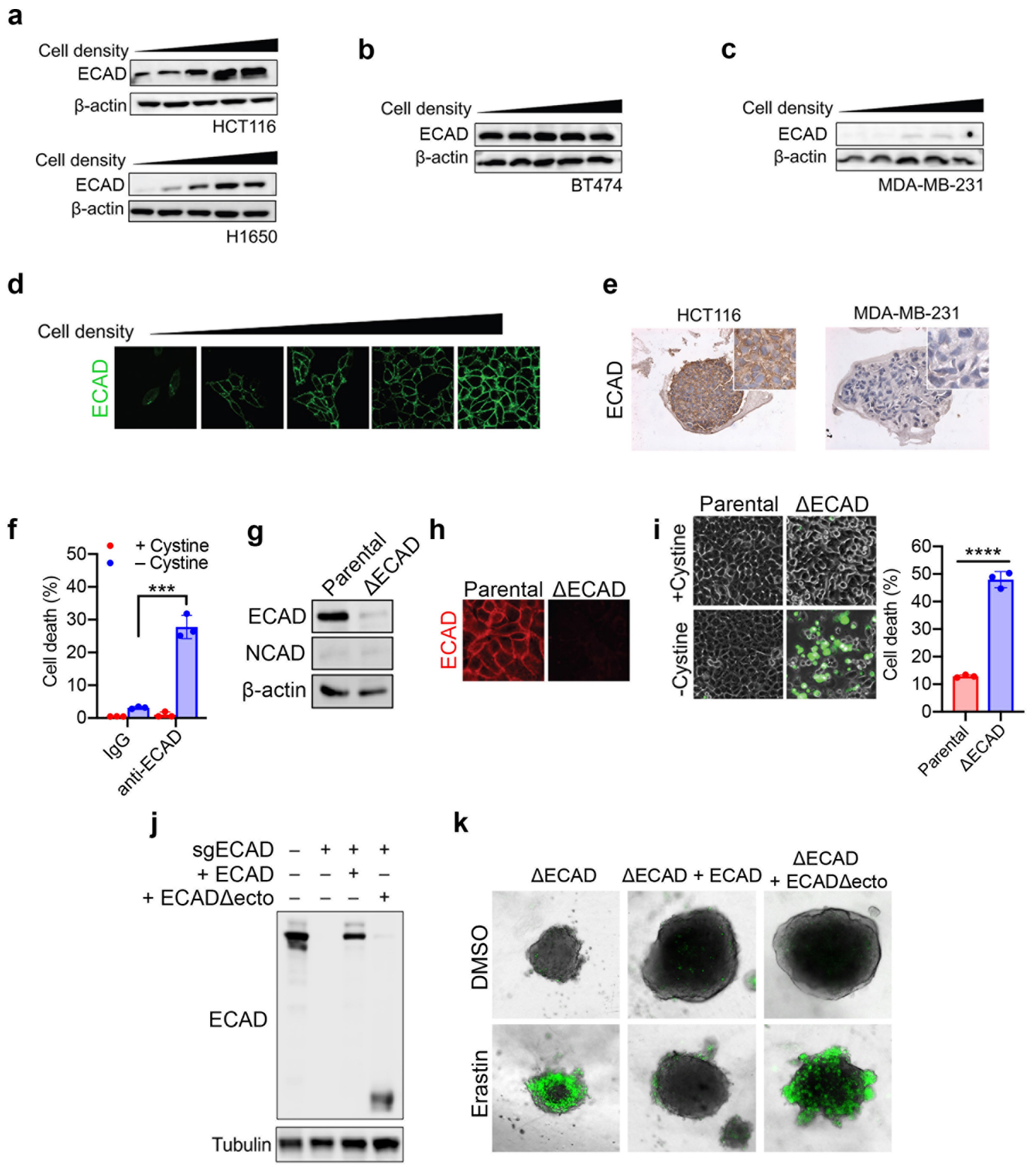

Extended Data Fig. 2 | See next page for caption.

Extended Data Fig. 2 | ECAD-mediated intercellular interaction regulates ferroptosis in a density-dependent manner. a, ECAD expression increases with cell density in HCT116 (top) and H1650 (bottom) cells. **b**, BT474 cells express high levels of ECAD regardless of cell density. **c**, MDA231 cells express low levels of ECAD regardless of cell density. **d**, Immunofluorescence of ECAD at increasing cell density in HCT116 cells (original magnification, ×200). **e**, Tumour spheroids generated from HCT116 or MDA231 cells were fixed, sectioned and stained for ECAD expression by immunohistochemistry (original magnification, ×100). **f**, HCT116 cells were treated with either IgG or an anti-ECAD antibody that blocks dimerization. Cell death was measured by propidium iodide staining followed by flow cytometry after cystine starvation for 30 h. ***$P = 0.0003$; two-tailed *t*-test. **g**, Western blot analysis of the expression of ECAD and NCAD in HCT116 cells after CRISPR–Cas9-mediated ECAD depletion (ΔECAD). **h**, ECAD depletion in HCT116 cells was further confirmed by immunofluorescence (magnification 200×). **i**, Cell death measurement of ΔECAD and the parental cell line seeded at a density of 4×10^5 cells per well after cystine starvation for 30 h. Original magnification, ×100. ****$P < 0.0001$; two tailed *t*-test. **j**, Western blot analysis confirming reconstitution of ECAD or ectodomain-truncated ECAD (ECADΔecto) into ECAD-depleted HCT116 cells. **k**, ΔECAD cells or ΔECAD cells re-expressing full-length ECAD or ECADΔecto were cultured into spheroids and treated with erastin for 30 h, followed by SYTOX Green staining to monitor cell death (magnification 100×). All data are mean ± s.d. from $n = 3$ biological replicates.

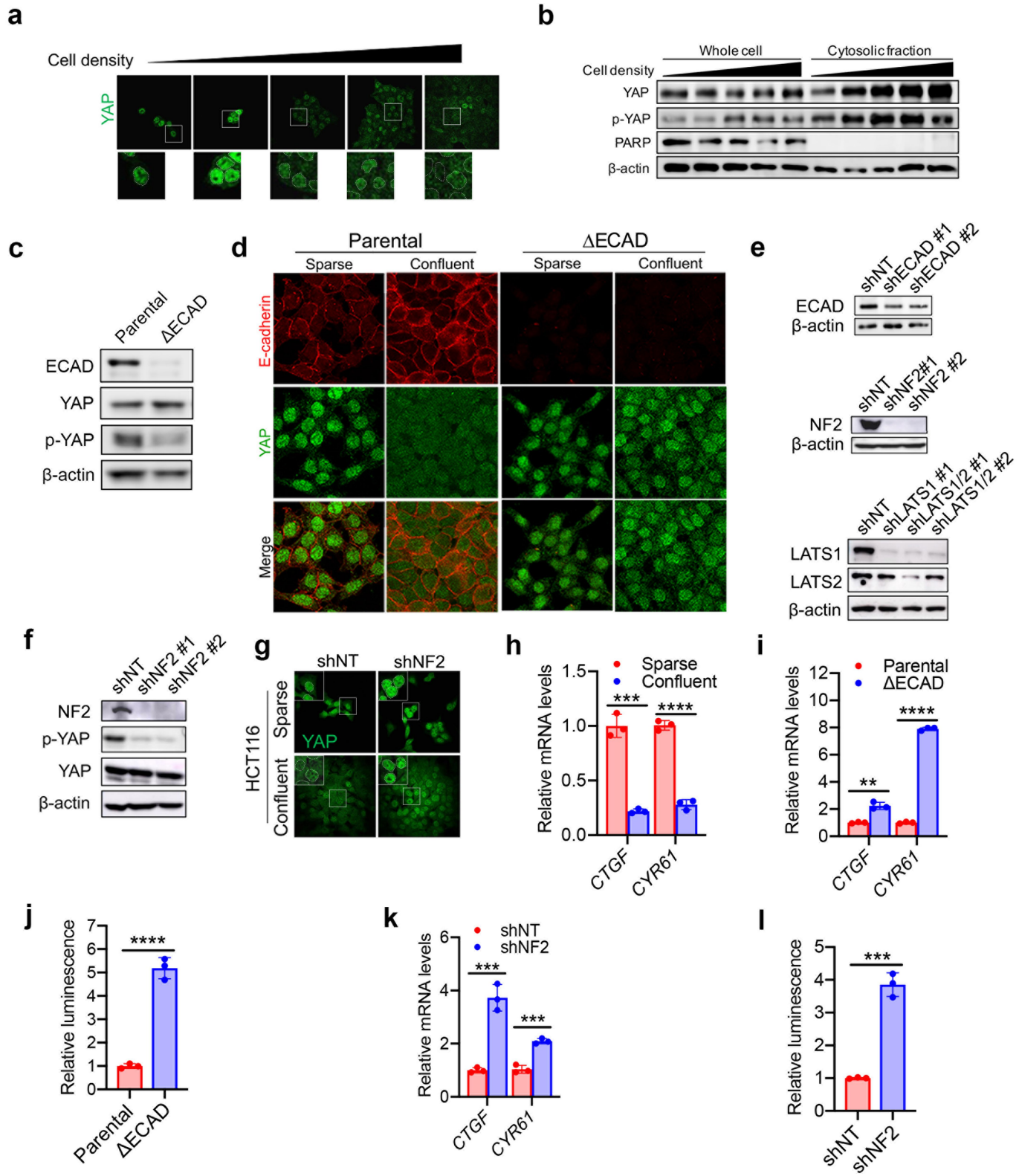

Extended Data Fig. 3 | See next page for caption.

Extended Data Fig. 3 | Cell density, ECAD and NF2 converge on the transcriptional co-regulator YAP. a, HCT116 cells were cultured at different cell densities and YAP localization was assessed by immunofluorescence. Original magnification, ×200. Bottom images are enlarged to show localization. **b**, Western blot analysis of phosphorylated YAP (p-YAP; at Ser127) and YAP in whole-cell or cytosolic fractions of HCT116 cells cultured at different densities. PARP was used as a marker for nuclear protein. **c**, Western blot analysis of ECAD, YAP and p-YAP in parental and ΔECAD HCT116 cells. **d**, Immunofluorescence of YAP (green) and ECAD (red) in parental and ΔECAD HCT116 cells. Original magnification, ×400. **e**, Western blot analysis confirming knockdown efficiency of ECAD (shECAD #1 and #2), NF2 (shNF2 #1 and #2), or LATS1 or LATS2 (shLATS1/2 #1 and #2, and shLATSs1 #1) in HCT116 cells. **f**, Western blot analysis of NF2, p-YAP and YAP in HCT116 cells transfected with shNT and shNF2. **g**, Knockdown of NF2 in HCT116 cells induced the nuclear accumulation of YAP in dense cell cultures, as assessed by immunofluorescence. Original magnification, ×200. **h**, Transcriptional levels of the canonical YAP targets *CTGF* and *CYR61* by qPCR in HCT116 cells seeded at 1×10^5 (sparse) or 8×10^5 (confluent) cells per well in 6-well dishes and grown for 24 h. $^{***}P = 0.0002$, $^{****}P < 0.0001$; two-tailed *t*-test. **i**, Transcription levels of *CTGF* and *CYR61* measured by qPCR in parental and ΔECAD HCT116 cells plated at high density. $^{**}P = 0.0013$, $^{****}P < 0.0001$; two-tailed *t*-test. **j**, YAP/TEAD transcriptional activity in HCT116 and ΔECAD cells was measured by a luciferase assay using the 8xGTIIC-luciferase reporter. $^{****}P < 0.0001$; two-tailed *t*-test. **k**, Transcription levels of *CTGF* and *CYR61* measured by qPCR in HCT116 cells plated at high density and transfected with shNT or shNF2. $^{***}P = 0.0007$, 0.0005 (left to right); two-tailed *t*-test. **l**, YAP/TEAD transcriptional activity in HCT116 cells transfected with shNT and shNF2 cells was measured by a luciferase assay using the 8xGTIIC-luciferase reporter. $^{***}P = 0.0002$; two-tailed *t*-test. All data are mean ± s.d. from $n = 3$ biological replicates.

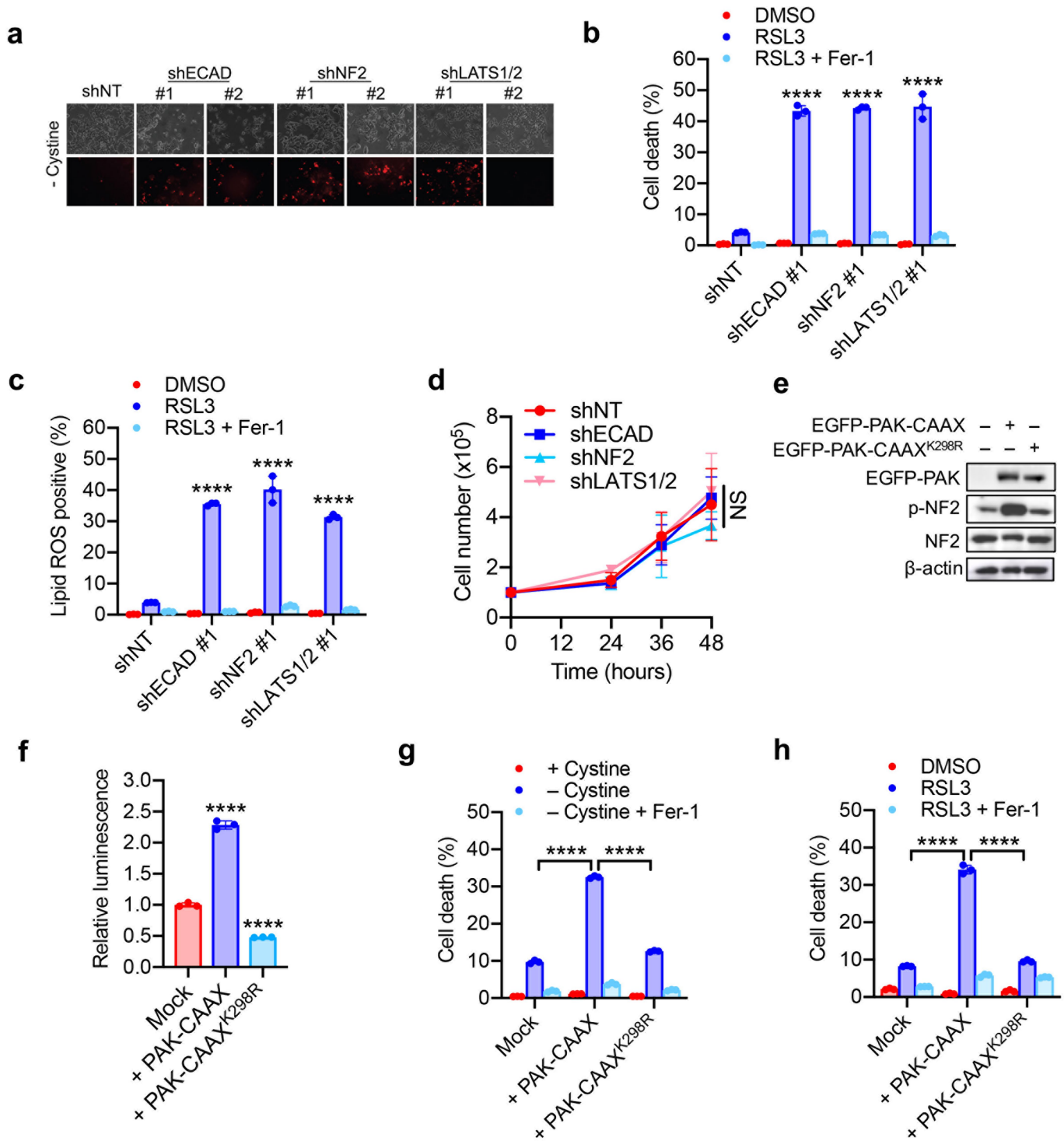

Extended Data Fig. 4 | The Hippo pathway links cell density and intercellular contact to ferroptosis. a, Confluent cells were subjected to cystine starvation for 30 h. Cell death was determined by propidium iodide staining. **b**, HCT116 cells expressing shNT, shECAD, shNF2 or shLATS1/2 as indicated were treated with 5 μM RSL3 with or without 2 μM Fer-1. Cell death was measured at 18 h. ****$P < 0.0001$; one-way ANOVA. **c**, Lipid ROS production of cells as in **b** was assessed at 12 h after treatment. ****$P < 0.0001$; one-way ANOVA. **d**, Cumulative cell growth curve expressed as the total cell count of HCT116 cells transfected with shNT, shECAD, shNF2 or shLATS1/2. n.s., $P = 0.9497$; two-way ANOVA. **e**, Western blot analysis of the expression and phosphorylation of NF2 in HCT116 cells transfected with enhanced green fluorescent protein (eGFP)-tagged PAK containing a prenylation (CAAX) motif (thus constitutively active), or an inactive mutant form of PAK (K298R). **f**, YAP/TEAD transcriptional activity was measured by a luminescence assay in HCT116 cells expressing activated or inactive PAK and transfected with the 8xGTIIC-luciferase reporter. ****$P < 0.0001$; one-way ANOVA. **g**, Cell death was measured in HCT116 cells plated at high density expressing activated or inactive PAK, and treated with cystine-free medium with or without 1 μM Fer-1 for 30 h. ****$P < 0.0001$; one-way ANOVA. **h**, Cells were prepared as in **g** and treated with DMSO or 5 μM RSL3 with or without 1 μM Fer-1. Cell death was measured at 24 h. ****$P < 0.0001$; one-way ANOVA. All data are mean ± s.d. from $n = 3$ biological replicates.

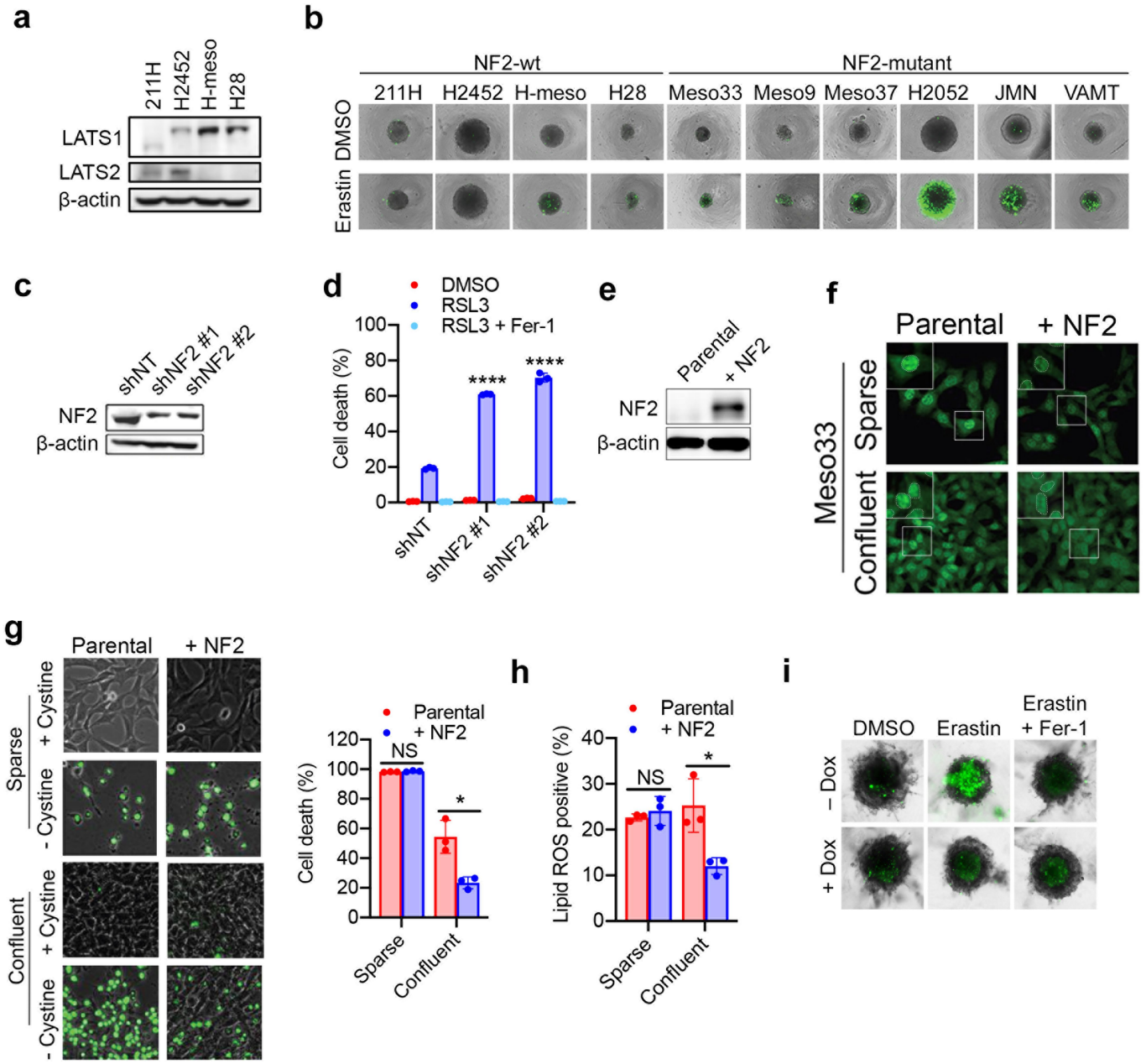

Extended Data Fig. 5 | NF2 expression correlates with sensitivity to ferroptosis in mesothelioma cell lines. a, Western blot analysis of the expression of LATS1 and LATS2 in the indicated mesothelioma cell lines. **b**, Spheroids were treated with 10 μM erastin for 24 h before SYTOX Green staining. Original magnification, ×40. **c**, Western blot analysis confirming knockdown efficiency of *NF2* shRNA in 211H cells. **d**, Confluent 211H cells transfected with shNT or shNF2 were treated with 1 μM RSL3, with or without 2 μM Fer-1. Cell death (left, 24 h after treatment) and lipid ROS production (right, 16 h) were measured. $^{****}P < 0.0001$; one-way ANOVA. **e**, NF2-mutant Meso33 cells were reconstituted with wild-type NF2, and the expression of NF2 was confirmed by western blot. **f**, Localization of YAP (green) under sparse or confluent conditions in Meso33 cells expressing wild-type NF2 was determined by immunofluorescence. Original magnification, ×200. **g**, Meso33 cells expressing wild-type NF2 were cultured under sparse or confluent conditions and stimulated with cystine-free medium. Cell death was measured by SYTOX Green staining coupled with flow cytometry after 24 h of treatment. Original magnification, ×100. n.s., $P = 0.1874$. $^{*}P = 0.0104$; two-tailed *t*-test. **h**, Meso33 cells expressing wild-type NF2 were cultured as in **g** and the production of lipid ROS was measured after cystine starvation for 16 h. n.s., $P = 0.4860$. $^{*}P = 0.0201$; two-tailed *t*-test. **i**, Meso33 spheroids containing Dox-inducible NF2 were grown in the presence or absence of 1 μg ml^{-1} Dox for 72 h, at which point 10 μM erastin was added. Cell death was measured after 24 h by SYTOX Green staining of spheroids. Original magnification, ×100. All data are mean ± s.d. from $n = 3$ biological replicates.

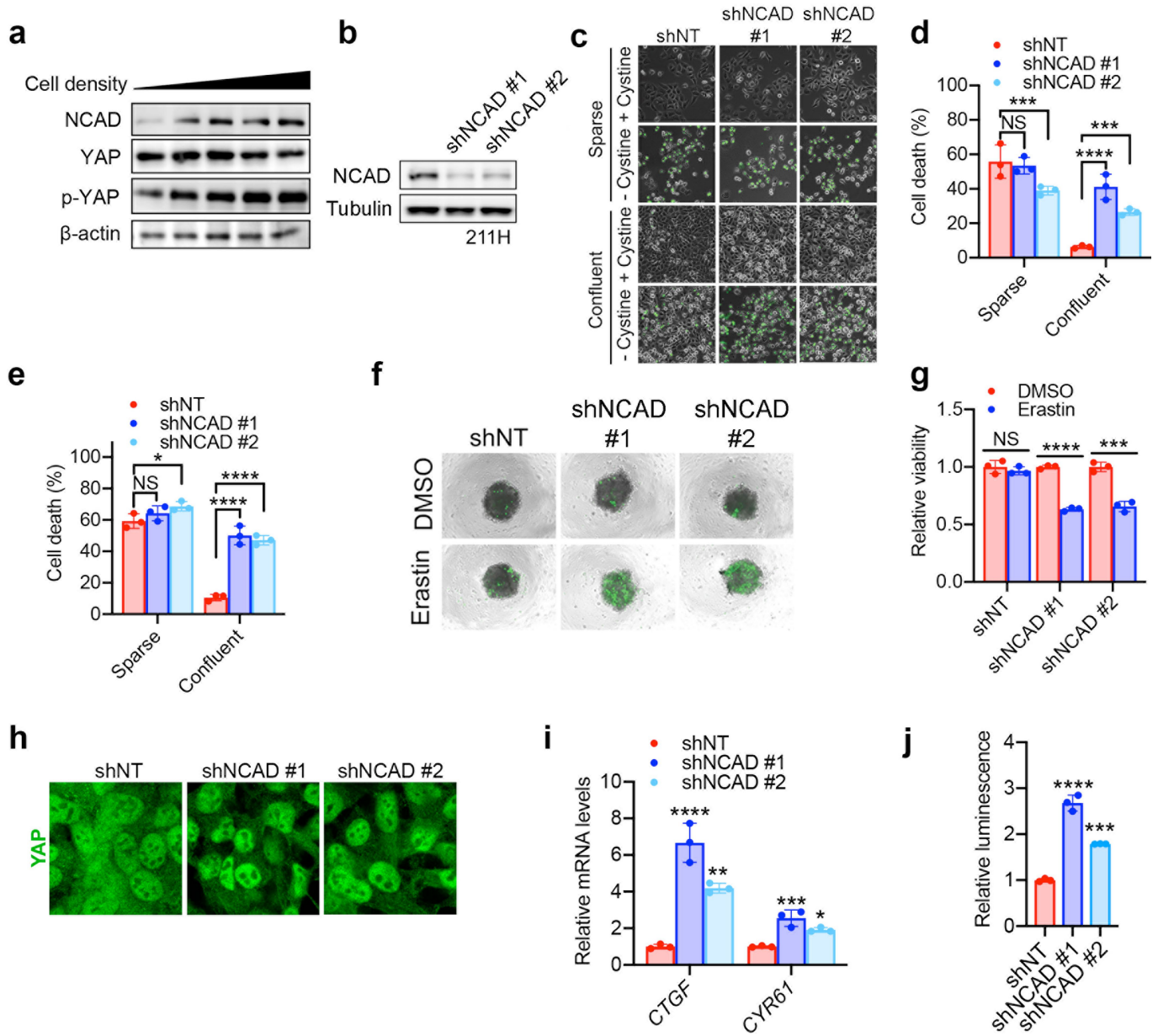

Extended Data Fig. 6 | NCAD suppresses ferroptosis in MSTO-211H cells in a density-dependent manner. a, Western blot analysis of the levels of NCAD, p-YAP and total YAP in 211H cells cultured at different cell densities. **b**, Knockdown efficiency of *NCAD* shRNA (shNcad #1 and #2) was assessed by western blot analysis in 211H cells infected with lentiviruses expressing shNCAD. **c**, Confluent or sparse shNT or shNCAD 211H cells, as indicated, were subjected to cystine starvation for 24 h, at which point cell death was monitored by SYTOX Green staining. Original magnification, ×100. **d**, Flow cytometric quantification of cell death in **c**. n.s., $P = 0.8426$. ***$P = 0.0056$, 0.0015 (left to right), ****$P < 0.0001$; one-way ANOVA. **e**, Confluent or sparse shNT or shNCAD 211H cells, as indicated, were treated with 1 μM RSL3 for 16 h, at which point cell death was measured by SYTOX Green staining followed by flow cytometry. n.s., $P = 0.3012$, *$P = 0.0315$, ****$P < 0.0001$; one-way ANOVA. **f**, Spheroids generated from shNT and shNCAD 211H cells were treated with 10 μM erastin for 24 h, and cell death was determined by SYTOX Green staining. Original magnification, ×40. **g**, Cell viability of spheroids described in **f** was assayed by measuring cellular ATP levels. n.s., $P = 0.4365$, ***$P = 0.0006$, ****$P < 0.0001$; two-tailed *t*-test. **h**, shNT or shNCAD 211H cells were plated at high density and YAP localization was assessed by immunofluorescence. Original magnification, ×400. **i**, Transcription levels of *CTGF* and *CYR61* measured by qPCR 211H cells plated at high density and transfected with shNT or shNCAD. *$P = 0.0108$, **$P = 0.0016$, ***$P = 0.0007$, ****$P < 0.0001$; one-way ANOVA. **j**, YAP/TEAD transcriptional activity in 211H cells transfected with shNT or shNCAD was measured by a luciferase assay using the 8xGTIIC-luciferase reporter. ***$P = 0.0002$, ****$P < 0.0001$; one-way ANOVA. All data are mean ± s.d. from $n = 3$ biological replicates.

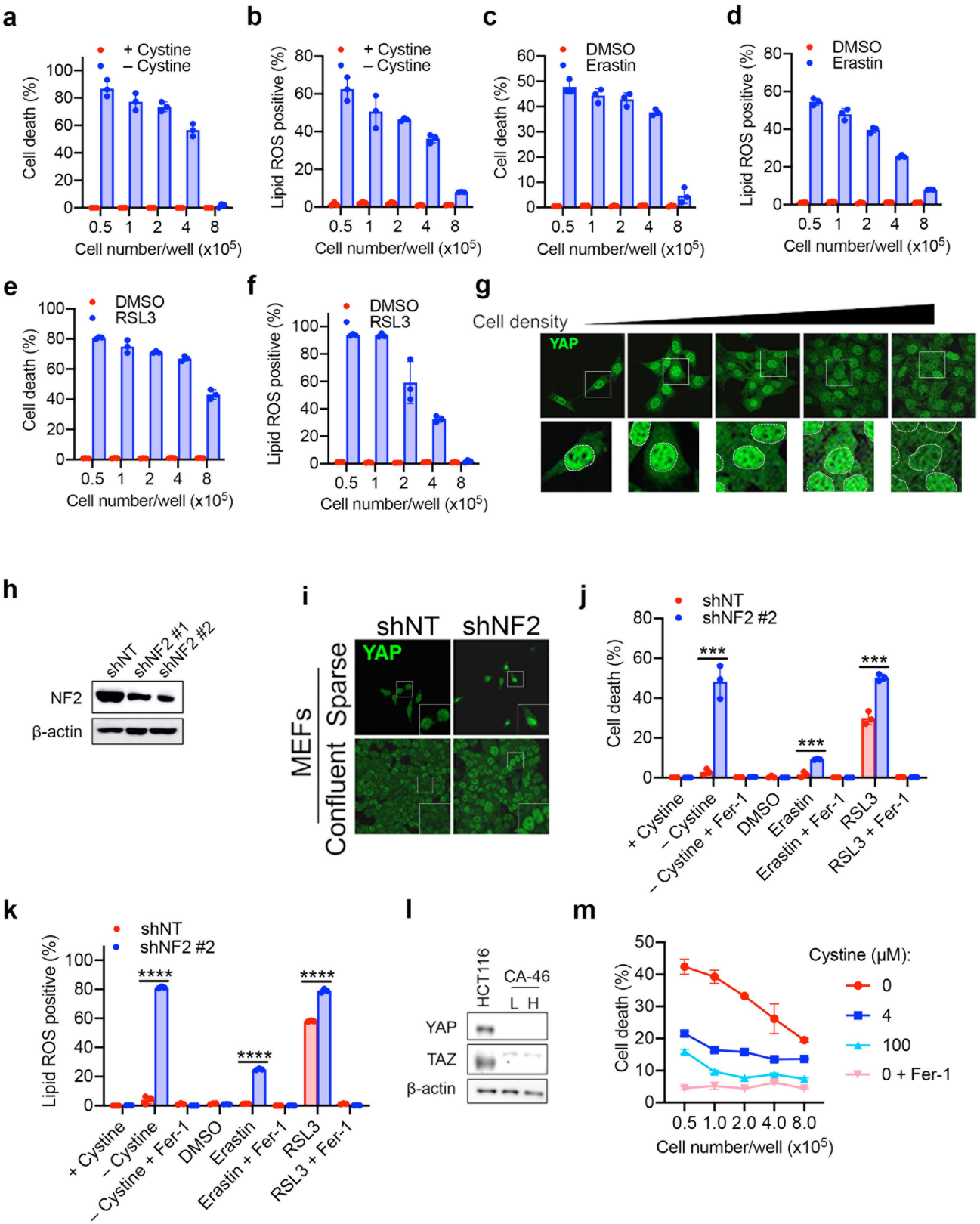

Extended Data Fig. 7 | See next page for caption.

Extended Data Fig. 7 | Ferroptosis can be regulated by the Hippo pathway in non-epithelial cells. a, Cell death was measured in MEFs after cystine starvation for 12 h. **b**, Cells were treated as in **a** and lipid ROS production was measured at 8 h. **c**, Cell death was measured in MEFs seeded at the indicated densities and treated with 1 μM erastin for 12 h. **d**, Cells were treated as in **c** and production of lipid ROS was measured at 8 h. **e**, MEFs treated with 1 μM RSL3 at the indicated densities were measured for cell death at 8 h. **f**, Cells were treated as in **e** and the production of lipid ROS was measured at 5 h. **g**, Immunofluorescence probing for YAP localization in MEFs seeded at increasing density. Bottom images are enlarged to show localization. Original magnification, ×400. **h**, MEFs were transfected with *NF2* shRNAs (shNF2 #1 and #2), and knockdown efficiency was assessed by western blot. **i**, Immunofluorescence probing for YAP localization after NF2 knockdown in MEFs. Original magnification, ×200. **j**, Increased cell death occurred in confluent MEFs after NF2 depletion (shNF2 #2) and cystine starvation, or treatment with erastin (1 μM, 12 h) or RSL3 (1 μM, 8 h), and this increase was blocked by Fer-1 (2 μM). ***$P = 0.0007$, 0.0007, 0.0006 (left to right); two-tailed *t*-test. **k**, Cells were treated as in **j** and lipid ROS production was assessed at 8 h (cystine starvation, erastin) or 5 h (RSL3). ****$P < 0.0001$; two-tailed *t*-test. **l**, Western blot analysis of expression of YAP and TAZ in CA-46 Burkitt lymphoma cells. **m**, Cell death measurement of CA-46 cells treated as indicated after 24 h. All data are mean ± s.d. from $n = 3$ biological replicates.

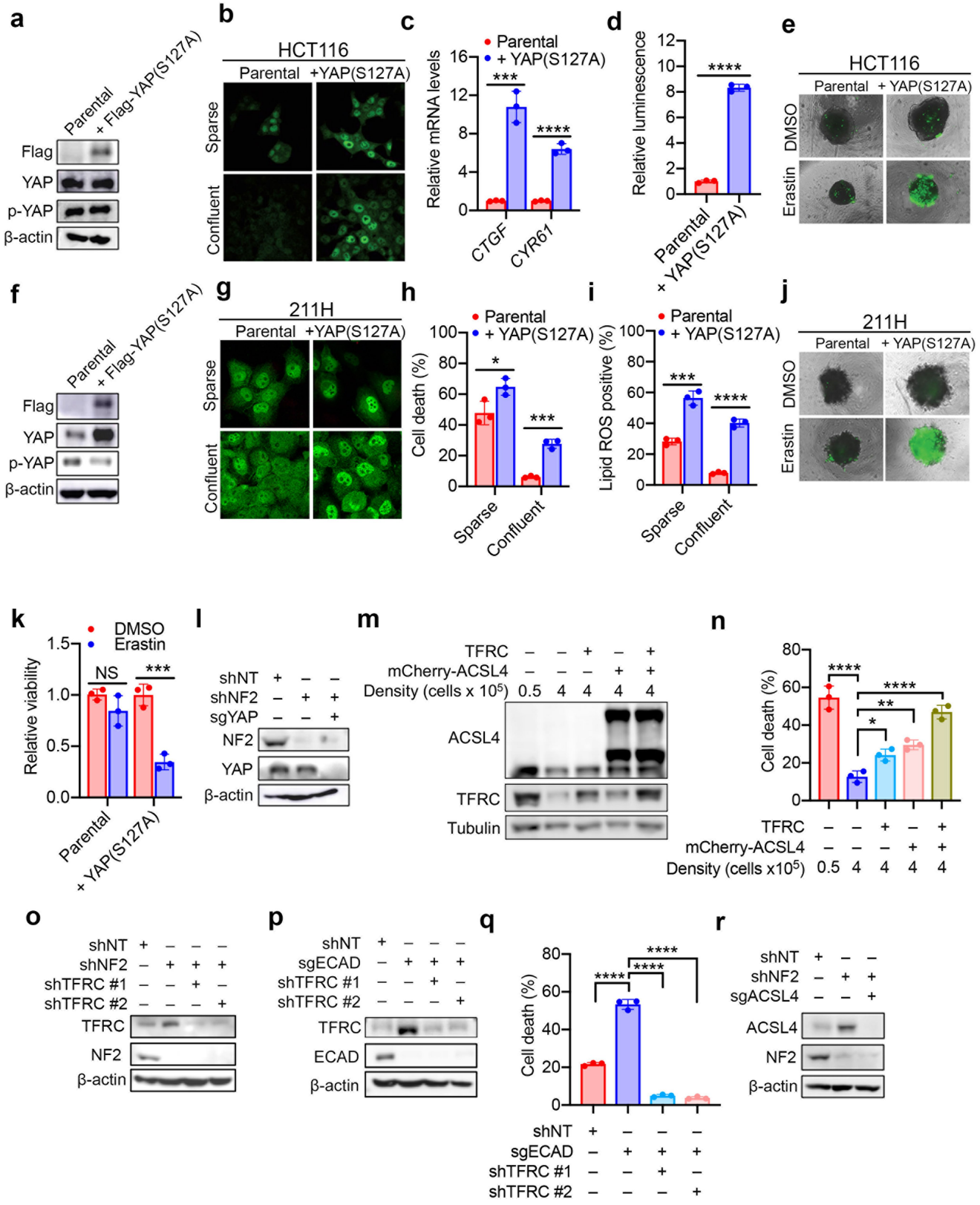

Extended Data Fig. 8 | See next page for caption.

Extended Data Fig. 8 | YAP regulates ferroptosis. a, Western blot confirming expression of YAP(S127A) in HCT116 cells. **b**, YAP localization in HCT116 cells expressing YAP(S127A) assessed by immunofluorescence. Original magnification, ×200. **c**, Transcriptional levels of *CTGF* and *CYR61* measured by qPCR in HCT116 cells expressing YAP(S127A). ***$P = 0.0005$, ****$P < 0.0001$; two-tailed *t*-test. **d**, YAP/TEAD transcriptional activity in HCT116 cells expressing YAP(S127A) was measured by a luminescence assay using the 8xGTIIC-luciferase reporter. ****$P < 0.0001$; two-tailed *t*-test. **e**, Spheroids generated from parental and YAP(S127A)-overexpressing HCT116 cells were treated with 15 μM erastin for 30 h, followed by SYTOX Green staining. Original magnification, ×40. **f**, 211H cells were infected with retroviral vectors encoding the Flag–YAP(S127A) mutant, and levels of Flag–YAP, YAP and p-YAP were analysed by western blot. **g**, Localization of YAP (green) was determined by immunofluorescence in 211H cells expressing constitutively active YAP. Original magnification, ×200. **h**, Parental and YAP(S127A)-overexpressing 211H cells were cultured under sparse or confluent conditions and cell death was measured after cystine starvation for 24 h. *$P = 0.0354$, ***$P = 0.0003$; two-tailed *t*-test. **i**, Cells were cultured as in **h** and the production of lipid ROS was measured after 16 h of cystine starvation. ***$P = 0.0006$, *** $P < 0.0001$; two-tailed *t*-test. **j**, Spheroids generated from parental and YAP(S127A)-overexpressing 211H cells were treated with 10 μM erastin for 24 h and cell death was measured by SYTOX staining. Original magnification, ×40. **k**, Cells were cultured as in **j** and cell viability within spheroids was determined by measuring cellular ATP levels. n.s., $P = 0.1534$. ***$P = 0.0009$l; two-tailed *t*-test. **l**, YAP was knocked out by CRISPR–Cas9 (sgYAP) in shNF2 HCT116 cells. **m**, HCT116 cells were transduced with retroviral particles containing mCherry–ACSL4 and/or transfected with TFRC. Expression levels were assayed by western blot. Two bands were detected for mCherry–ACSL4, representing the full-length mCherry–ACSL4 and that with the mCherry tag truncated. **n**, HCT116 cells treated as in **m** were plated at the indicated density and treated with 2 μM RSL3 for 24 h. Cell death was measured by SYTOX Green staining coupled with flow cytometry. *$P = 0.0158$, **$P = 0.0012$, ****$P < 0.0001$; one-way ANOVA. **o**, Western blot analysis confirming knockdown of TFRC in HCT116 shNF2 cells. **p**, Western blot confirming knockdown of TFRC in HCT116 ΔECAD (sgECAD) cells. **q**, Cells as in **p** were treated with medium lacking cystine for 30 h. Cell death was measured by SYTOX Green staining coupled with flow cytometry. ****$P < 0.0001$; one-way ANOVA. **r**, Western blot analysis of HCT116 cells after CRISPR–Cas9-mediated knockout of ACSL4 (sgACSL4) and/or transfection with shNF2. All data are mean ± s.d. from $n = 3$ biological replicates.

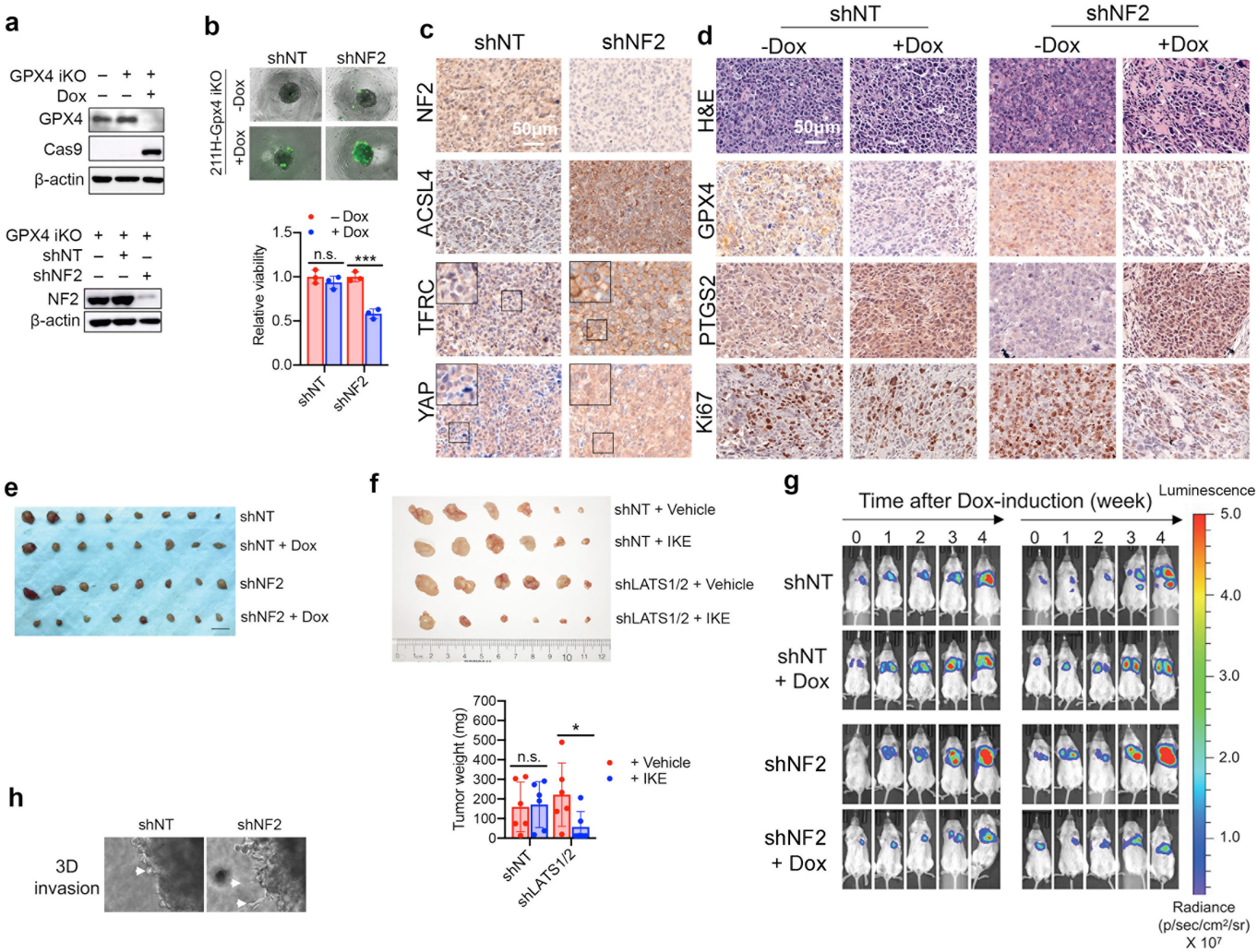

Extended Data Fig. 9 | NF2, LATS1 and LATS2 regulate cancer cell sensitivity to ferroptosis in vivo. a, Top, western blot analysis confirming knockout of GPX4 (GPX4 iKO) in 211H cells after treatment with 1 μg ml^{-1} Dox for 5 days (top). Bottom, cells were infected with the indicated hairpins. **b**, Spheroids formed by shNT-GPX4-iKO or shNF2-GPX4-iKO 211H cells were treated with or without Dox for five days. Cell death and viability, respectively, were determined by SYTOX staining (top) and cellular ATP levels (bottom). Original magnification, ×40. n.s., $P = 0.3523$, $^{***}P = 0.0007$; two-tailed *t*-test. **c**, shNT-GPX4-iKO and shNF2-GPX4-iKO cells were subcutaneously injected into nude mice. The effect of NF2 knockdown on xenografted tumours was validated by immunostaining of NF2, ACSL4, TFRC and YAP, all counterstained with haematoxylin (blue), on sections of tumours bearing shNT and shNF2 as indicated. Inset images are enlarged to show TFRC expression at plasma membranes and increase in nuclear localization of YAP. **d**, shNT-GPX4-iKO cells and shNF2-GPX4-iKO cells were subcutaneously injected into nude mice followed by treatment with or without Dox (to induce GPX4 knockout; $n = 8$ mice per group). Representative haematoxylin and eosin (H&E) and immunostaining images of GPX4, PTGS2 and Ki67, all counterstained with haematoxylin (blue), are shown from sections of xenografted tumours. **e**, Images of resected MSTO-211H subcutaneous tumours. Scale bar, 1 cm. **f**, Mice injected subcutaneously with HCT116 cells expressing shNT or shLATS1/2 as indicated were treated with or without IKE. Top, images of resected HCT116 shNT or shLATS1/2 tumours. Bottom, mass of resected tumours. $n = 6$ mice per group. n.s., $P = 0.8677$. $^{*}P = 0.0486$; two-tailed *t*-test. **g**, Representative BLI showing the tumour growth of indicated cells in an orthotopic model of mesothelioma in nonobese diabetic/severe combined immunodeficiency (NOD/SCID) mice. Dox treatment started when the average total flux reached 10^8 photons per second (time point 0). **h**, Tumour spheroids of 211H cells expressing shNT or shNF2 were grown in Matrigel, and invasion was monitored. In the representative images, arrows show protrusions extruded from the main body of spheroids. Original magnification, ×400. All data are mean ± s.d. from $n = 3$ biological replicates.

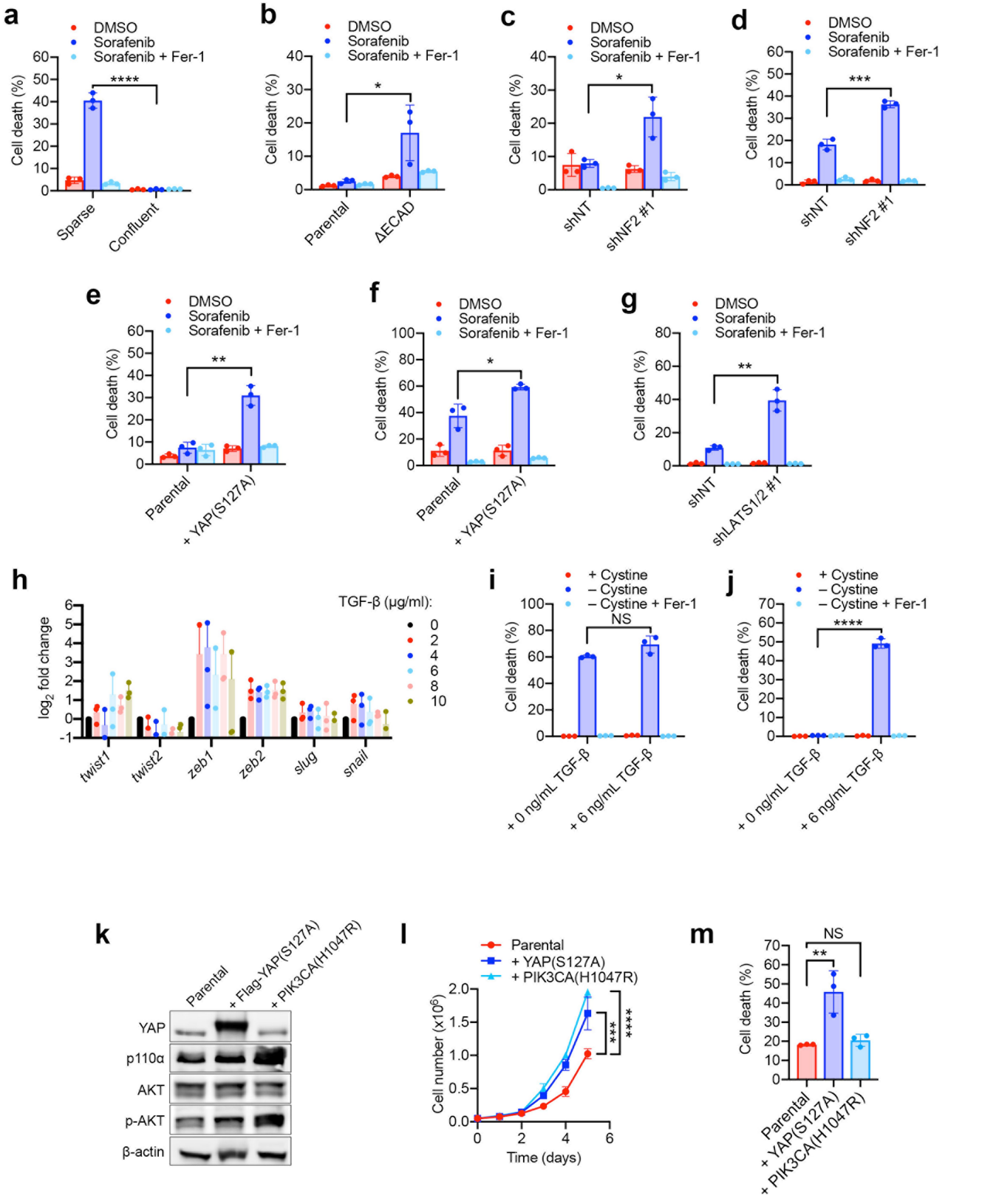

Extended Data Fig. 10 | See next page for caption.

Extended Data Fig. 10 | The Hippo pathway as a potential biomarker for predicting cancer cell sensitivity to ferroptosis. a, Cell death was measured in HCT116 cells seeded at 0.5×10^5 cells per 3.5 cm^2 well (sparse) or 4×10^5 cells per 3.5 cm^2 well (confluent) and grown for 24 h. Cells were treated with DMSO, 10 μM sorafenib or 10 μM sorafenib plus 2 μM Fer-1 as indicated for 24 h. $^{****}P < 0.0001$; two-tailed *t*-test. **b**, Cell death was measured in parental or ΔECAD HCT116 cells seeded at 4×10^5 cells per 3.5 cm^2 well and grown for 24 h. Cells were treated as in **a**. $^{*}P = 0.0394$; two-tailed *t*-test. **c**, **d**, Cell death was measured in HCT116 (**c**) or 211H (**d**) shNT or shNF2 cells seeded at high density and treated as in **a**. $^{*}P = 0.0167$, $^{***}P = 0.0004$; two-tailed *t*-test. **e**, **f**, Cell death was measured in HCT116 (**e**) or 2211H (**f**) cells expressing parental or YAP(S127A) cells seeded at high density and treated as in **a**. $^{*}P = 0.0143$, $^{**}P = 0.0014$; two-tailed *t*-test. **g**, Cell death was measured in HCT116 shNT or shLATS1/2 cells seeded at high density and treated as in **a**. $^{**}P = 0.0017$; two-tailed *t*-test. **h**, NF639 cells, derived from mouse mammary tumours containing MMTV-neu, were treated with various concentrations of TGFβ for 48 h. mRNA expression of a panel of EMT-related genes was assayed by qPCR. **i**, NF639 cells were treated with or without 6 ng μl^{-1} TGFβ for 48 h, at which point they were plated at low density (0.8×10^5 cells per 3.5 cm^2 well), grown overnight and treated with medium containing or lacking cystine, with or without 1 μM Fer-1 for 12 h, followed by cell death measurement. n.s., $P = 0.0777$; two-tailed *t*-test. **j**, NF639 cells were plated at 3.2×10^5 cells per 3.5 cm^2 well, grown overnight and treated as described in **a**. $^{****}P < 0.0001$; two-tailed *t*-test. **k**, 211H cells were infected with YAP(S127A) or the activated mutant PIK3CA(H1047R). Lysates were probed for overexpression and phosphorylated AKT (p-AKT; S473) to confirm the activity of PIK3CA(H1047R). **l**, Approximately 50,000 211H cells were seeded in 3.5-cm^2 plates and grown for 5 days. Cells were counted daily. $^{***}P = 0.0007$, $^{****}P < 0.0001$; two-way ANOVA. **m**, Cell death was measured by flow cytometry in 211H cells seeded at high density (8×10^5 cells per 3.5-cm^2 well) after cystine starvation for 24 h. n.s., $P = 0.8838$. $^{**}P = 0.0041$; one-way ANOVA. All data are mean ± s.d.; $n = 3$ biological replicates.

nature research

Corresponding author(s): Xuejun Jiang, Zhi-Nan Chen

Last updated by author(s): May 8, 2019

Reporting Summary

Nature Research wishes to improve the reproducibility of the work that we publish. This form provides structure for consistency and transparency in reporting. For further information on Nature Research policies, see Authors & Referees and the Editorial Policy Checklist.

Statistics

For all statistical analyses, confirm that the following items are present in the figure legend, table legend, main text, or Methods section.

n/a	Confirmed	
☐	☒	The exact sample size (*n*) for each experimental group/condition, given as a discrete number and unit of measurement
☐	☒	A statement on whether measurements were taken from distinct samples or whether the same sample was measured repeatedly
☐	☒	The statistical test(s) used AND whether they are one- or two-sided *Only common tests should be described solely by name; describe more complex techniques in the Methods section.*
☐	☒	A description of all covariates tested
☐	☒	A description of any assumptions or corrections, such as tests of normality and adjustment for multiple comparisons
☐	☒	A full description of the statistical parameters including central tendency (e.g. means) or other basic estimates (e.g. regression coefficient) AND variation (e.g. standard deviation) or associated estimates of uncertainty (e.g. confidence intervals)
☐	☒	For null hypothesis testing, the test statistic (e.g. *F*, *t*, *r*) with confidence intervals, effect sizes, degrees of freedom and *P* value noted *Give P values as exact values whenever suitable.*
☒	☐	For Bayesian analysis, information on the choice of priors and Markov chain Monte Carlo settings
☒	☐	For hierarchical and complex designs, identification of the appropriate level for tests and full reporting of outcomes
☒	☐	Estimates of effect sizes (e.g. Cohen's *d*, Pearson's *r*), indicating how they were calculated

Our web collection on statistics for biologists contains articles on many of the points above.

Software and code

Policy information about availability of computer code

Data collection	BD FACSDiva (v8.0.1) was used to collect flow cytometry data. Tecan iControl software (v1.12) was used for the collection of viability/luminescence data in cultured cells. In vivo imaging studies were performed using Caliper Life Sciences Living Image software (v4.3.1).
Data analysis	BD FACSDiva (v8.0.1) and FlowJo (v10.0.7) were used for analysis of flow cytometry data. GraphPad Prism (v7.0) was used for statistical analysis of all data.

For manuscripts utilizing custom algorithms or software that are central to the research but not yet described in published literature, software must be made available to editors/reviewers. We strongly encourage code deposition in a community repository (e.g. GitHub). See the Nature Research guidelines for submitting code & software for further information.

Data

Policy information about availability of data

All manuscripts must include a data availability statement. This statement should provide the following information, where applicable:

- Accession codes, unique identifiers, or web links for publicly available datasets
- A list of figures that have associated raw data
- A description of any restrictions on data availability

All data generated or analysed during this study are included in the manuscript and supplementary information files.

Field-specific reporting

Please select the one below that is the best fit for your research. If you are not sure, read the appropriate sections before making your selection.

☒ Life sciences ☐ Behavioural & social sciences ☐ Ecological, evolutionary & environmental sciences

Life sciences study design

All studies must disclose on these points even when the disclosure is negative.

Sample size	No statistical calculations were performed to predetermine sample size.
Data exclusions	No data has been excluded from this study.
Replication	All experiments presented in this study yielded reproducible results for a minimum of three independent replicates.
Randomization	For animal experiments, animals, were randomized for testing different conditions.
Blinding	Animal studies were blinded for the collection of measurements.

Reporting for specific materials, systems and methods

We require information from authors about some types of materials, experimental systems and methods used in many studies. Here, indicate whether each material, system or method listed is relevant to your study. If you are not sure if a list item applies to your research, read the appropriate section before selecting a response.

Materials & experimental systems

n/a	Involved in the study
☐	☒ Antibodies
☐	☒ Eukaryotic cell lines
☒	☐ Palaeontology
☐	☒ Animals and other organisms
☒	☐ Human research participants
☒	☐ Clinical data

Methods

n/a	Involved in the study
☒	☐ ChIP-seq
☐	☒ Flow cytometry
☒	☐ MRI-based neuroimaging

Antibodies

Antibodies used	Western blots: GPX4 (Abcam, ab125066, GR251529-31, [EPNCIR144], 1:1000); E-cadherin (Abcam, ab76055, GR317373-2, [M168], 1:1000); N-cadherin (Abcam, ab76057, GR259225-14, polyclonal, 1:1000); pan-cadherin (Cell Signaling, 4086T, 2, polyclonal, 1:1000); Merlin (Cell Signaling, 12888S, 1, [D3S3W], 1:1000); pMerlin-Ser518 (Cell Signaling, 13281, 1, [D5A4I], 1:1000); LATS1 (Cell Signaling, 3477T, 7, [C66B5], 1:1000); LATS2 (Cell Signaling, 5888S, [D83D6], 1:1000); YAP (Cell Signaling, 14074S, 2, [D8H1X], 1:1000); pYAP-Ser127 (Cell Signaling, 4911S, 5, polyclonal, 1:1000); ACSL4 (Thermo Fisher, PA5-27137, polyclonal, 1:1000); transferrin receptor (Abcam, ab214039, GR189553-8, polyclonal, 1:1000); TAZ (Cell Signaling, 83669S, 1, [E8E9G], 1:1000); p110 alpha (Cell Signaling, 4249S, 7, [C73F8], 1:1000); AKT (Cell Signaling (2920S, 16, [40D4], 1:1000); pAKT-Ser473 (Cell Signaling, 4060S, 3, D9E, 1:1000); Cas9 (Cell Signaling, 14697S, 3, [7A9-3A3], 1:1000); HA (Sigma-Aldrich, H3663, [HA-7], 1:2000); Flag (Sigma-Aldrich, F1804, SLBW3851, [M2], 1:2000); GFP (Invitrogen, A11122, 1024102, polyclonal, 1:3000); alpha tubulin (Calbiochem, CP06, D00175772, [DM1A], 1:3000); beta actin (Sigma-Aldrich, A1978, [AC-15], 1:3000); rabbit IgG-HRP (Thermo Fisher, 31458, polyclonal, 1:10000); mouse IgG-HRP (Thermo Fisher, 31430, polyclonal, 1:10000). Immunofluorescence: E-cadherin (Abcam, ab76055, GR317373-2, [M168], 1:200); YAP (Cell Signaling, 14074S, 2, [D8H1X], 1:200); rabbit IgG-AlexaFluor488 (Invitrogen, A11008, 34732A, polyclonal, 1:500); rabbit IgG-AlexaFluor594 (Invitrogen, A11012, 1810936, polyclonal, 1:500); mouse IgG-AlexaFluor488 (Invitrogen, A11029, 673781, polyclonal, 1:500); mouse IgG-AlexaFluor594 (Invitrogen, A11005, 610868, polyclonal, 1:500). Immunohistochemistry: GPX4 (Abcam, ab125066, GR251529-31, [EPNCIR144], 1:100); YAP (Cell Signaling, 14074S, 2, [D8H1X], 1:400); ACSL4 (Thermo Fisher, PA5-27137, polyclonal, 1:200); transferrin receptor (Abcam, ab214039, GR189553-8, polyclonal, 1:400); Merlin (Abcam, ab88957, GR310755-14, [AF1G4], 1:100); PTGS2 (Cell Signaling, 12282, 4, [D5H5], 1:400); Ki67 (Cell Signaling, 9449, 4, [8D5], 1:400). ChIP: TEAD4 (Abcam, ab58310, GR3205108-1, 10 µg/sample)
Validation	Antibodies were only used for applications and organisms verified by the manufacturer.

Eukaryotic cell lines

Policy information about cell lines

Cell line source(s)	MEF, HEK293T, HepG2, H1650, BT474, MDA-MB-231, NF639, and CA-46 cells were acquired from ATCC. PC9 cells were acquired from Sigma-Aldrich. The human mesothelioma cell lines 211H, H2452, H28, H-meso, Meso33, Meso9, Meso37,

	H2052, JMN, and VAMT were a gift from the lab of Filippo Giancotti (MD Anderson, Houston, TX). 211H, H2452, H28, and H2052 are available on ATCC.
Authentication	All ATCC cell lines were authenticated by STR DNA profiling analysis through ATCC. All other cell lines were also profiled through STR analysis and found to not match any cell line available from ATCC.
Mycoplasma contamination	All cell lines tested negative for mycoplasma contamination.
Commonly misidentified lines (See ICLAC register)	No cell lines used in this study are listed in the ICLAC database.

Animals and other organisms

Policy information about studies involving animals; ARRIVE guidelines recommended for reporting animal research

Laboratory animals	Athymic nude mice: female, 6-8 weeks. Nod/SCID mice: female, 6-8 weeks.
Wild animals	This study did not involve wild animals.
Field-collected samples	This study did not involve field-collected samples.
Ethics oversight	All protocols used in this study were approved by the Memorial Sloan Kettering Institutional Animal Care and Use Committee (IACUC).

Note that full information on the approval of the study protocol must also be provided in the manuscript.

Flow Cytometry

Plots

Confirm that:

☒ The axis labels state the marker and fluorochrome used (e.g. CD4-FITC).

☒ The axis scales are clearly visible. Include numbers along axes only for bottom left plot of group (a 'group' is an analysis of identical markers).

☒ All plots are contour plots with outliers or pseudocolor plots.

☒ A numerical value for number of cells or percentage (with statistics) is provided.

Methodology

Sample preparation	All cells used in Flow Cytometry are cultured cell lines. Cell death was analyzed by propidium iodide (Invitrogen, Waltham, MA, USA) or SYTOX Green (Invitrogen) staining followed flow cytometry. Samples were washed with PBS before flow cytometry. To analyze lipid peroxidation, cells were stained 5 µM BODIPY-C11 (Invitrogen) for 30 minutes at 37°C followed by flow cytometric analysis.
Instrument	LSRII (BD Biosciences)
Software	BD FACSDiva (v8.0.1) was used to collect data, BD FACSDiva (v8.0.1) and Flowjo (v10.0.7) were used to analyze the data.
Cell population abundance	For all samples, a minimum of 10,000 cells were collected.
Gating strategy	For cell death detection, unstained controls (PBS alone without staining) were used as negative control. The first plot (FSC-A vs. SSC-A) was drawn to exclude debris as they tend to have lower forward scatter levels. The second and third plots (SSC-W vs. SSC-H and FSC-W vs. FSC-H) are drawn to remove doublets from the analysis. Then a single parameter histogram was used to identify cells which would be positive for the dye. A gate boundary is made based on the unstained cells and the peaks of the histogram. For lipid ROS staining, samples without BODIPY-C11 was used as negative control. A figure exemplifying the gating strategy are provided in Supplementary information.

☒ Tick this box to confirm that a figure exemplifying the gating strategy is provided in the Supplementary Information.